

~~CONFIDENTIAL~~Copy 6  
RM L53J22a

NACA RM L53J22a

**NACA****RESEARCH MEMORANDUM**

INVESTIGATION AT TRANSONIC SPEEDS OF AERODYNAMIC  
CHARACTERISTICS OF A SEMIELLIPTICAL AIR INLET  
IN THE ROOT OF A 45° SWEEPBACK WING

By Robert R. Howell and Charles D. Trescot, Jr.

Langley Aeronautical Laboratory  
Langley Field, Va.  
**CLASSIFICATION CHANGED**  
**UNCLASSIFIED**

**LIBRARY COPY**

DEC 16 1953

LANGLEY AERONAUTICAL LABORATORY  
LIBRARY, NACA  
LANGLEY FIELD, VIRGINIA

Authority of *NACA Review* *effective*  
*PRN-121* *Oct. 14, 1957*

Date

AMF 11-15 57

CLASSIFIED DOCUMENT

This material contains information affecting the National Defense of the United States within the meaning of the espionage laws, Title 18, U.S.C., Sec. 793 and 794, the transmission or revelation of which in any manner to an unauthorized person is prohibited by law.

**NATIONAL ADVISORY COMMITTEE  
FOR AERONAUTICS**

WASHINGTON

December 11, 1953

~~CONFIDENTIAL~~



## NATIONAL ADVISORY COMMITTEE FOR AERONAUTICS

## RESEARCH MEMORANDUM


INVESTIGATION AT TRANSONIC SPEEDS OF AERODYNAMIC  
CHARACTERISTICS OF A SEMIELLIPTICAL AIR INLET  
IN THE ROOT OF A  $45^\circ$  SWEEPBACK WING

By Robert R. Howell and Charles D. Trescot, Jr.

## SUMMARY

An investigation has been made in the Langley transonic blowdown tunnel at Mach numbers from 0.63 to 1.41 to determine the increments in lift, drag, and pitching moments due to the installation of a semielliptical-shaped air inlet in the root of a  $45^\circ$  sweptback wing and to study the internal flow characteristics of the inlet. The test ranges of angle of attack and mass-flow ratio varied from  $0^\circ$  to  $9.6^\circ$  and 0.3 to 0.86, respectively.

At an inlet mass-flow ratio of 0.80, a maximum total-pressure recovery of 0.97 was obtained up to a Mach number of 1.0. The total-pressure recovery decreased with increasing supersonic Mach number to a value of 0.90 at a Mach number of 1.40. The recovery increased rather rapidly with increasing inlet mass-flow ratio for Mach numbers above about 1.10. Removal of only about 3 percent of the inlet air through a boundary-layer removal scoop increased the subsonic total-pressure recovery 0.5 percent and the total-pressure recovery at Mach numbers of 1.25 and 1.40, 3.5 percent and 2.0 percent, respectively, for angles of attack of  $0^\circ$  and  $4.2^\circ$ . The changes in external aerodynamic characteristics due to installation of the inlet were generally small. A maximum increase in drag coefficient of about 0.005 occurred at an angle of attack of about  $4^\circ$ . The primary effect of the inlet installation on the pitching moments was an increase in longitudinal stability in a Mach number range near 1.0. At low angles of attack, the performance of the triangular-shaped wing-root air inlet investigated in NACA RM L52H08a was comparable with that of the present inlet. At an angle of attack of about  $4^\circ$ , the semielliptical-inlet performance was higher due primarily to a lower inlet drag. Further improvement in performance of wing-root inlets appears to depend largely on the development of an efficient boundary-layer removal system.



## INTRODUCTION

The results of tests of a triangular-shaped wing-root air inlet (ref. 1) indicated that this type of inlet has performance characteristics comparable with those of the nose and fuselage scoop inlet in the transonic speed range. In addition to leaving the nose of the aircraft free to house radar, armament, and so forth, it has also been found in some cases that thickening the wing root to allow installation of a wing-root type inlet may be advantageous in improving the structural qualities of the inboard wing sections thereby reducing the structural weight required to withstand a given bending moment.

The triangular-shaped wing-root inlet of reference 1 was developed at low speeds (ref. 2). Upon testing it at transonic speeds, it was found to have certain unfavorable internal-flow characteristics resulting from excessive inlet lip droop and stagger. It was also believed that the transition of the internal duct from the triangular to semicircular cross section over the limited duct length led to excessive duct losses and flow nonuniformity at the compressor face measuring station.

As a consequence of these findings, another wing-root inlet was designed. This inlet was semielliptical in shape, had no inlet lip droop, and had reduced lip stagger, especially of the outboard sections of the inlet. The internal duct cross-sectional transition was smooth and more gradual compared with the triangular inlet of reference 1.

It is the purpose of the present paper to present the results of a transonic investigation of the semielliptical inlet. The investigation included measurements of the changes in external aerodynamic forces due to the inlet installation and the internal-flow characteristics of the inlet. A basic unducted model was used for comparative purposes. One design of a boundary-layer removal system was tested to obtain the effect of boundary-layer removal on pressure recovery.

## SYMBOLS

$C_{D_b}$	basic model drag coefficient, $\frac{\text{Drag}}{q_0 S}$
$\Delta C_{D_{\text{ext}}}$	difference in drag coefficient obtained between inlet and basic configurations at same angle of attack and Mach number after effects of air exit have been removed (appendix, see ref. 1)

- $C_{L_b}$  basic model lift coefficient,  $\frac{\text{Lift}}{q_0 S}$
- $\Delta C_{L_{\text{ext}}}$  difference in lift coefficient obtained between inlet and basic configurations at same angle of attack and Mach number after effects of air exit have been removed (appendix, see ref. 1)
- $C_{m_b}$  basic model pitching-moment coefficient taken about quarter-chord position of the mean aerodynamic chord,  $\frac{\text{Moment}}{q_0 \bar{c}}$
- $\Delta C_m$  difference in pitching-moment coefficient obtained between inlet and basic configurations at constant lift coefficient and Mach number after effects of air-exit installation have been removed
- $C_{T_{\text{ideal}}}$  engine thrust coefficient based on ideal conditions  $\frac{\bar{H}}{H_0} = 1.0$
- $\bar{H}/H_0$  integrated total-pressure recovery weighted with respect to mass flow, 
$$\frac{\int_A \frac{\rho V}{\rho_0 V_0} \left( \frac{H}{H_0} \right) dA}{\int_A \frac{\rho V}{\rho_0 V_0} dA}$$
- $\frac{H - p_0}{H_0 - p_0}$  impact pressure ratio
- $m_1/m_0$  mass-flow ratio, defined as ratio of total internal mass flow to mass flow through a free-stream tube equal in area to that of projected area of inlet
- $A$  area
- $A_1$  projected frontal areas of both inlet openings normal to flow direction, defined by maximum inner lip radius and fuselage wall
- $A_{\text{min}}$  minimum cross-sectional area of duct located at inlet measuring station (see fig. 2)
- $c$  local chord

$\bar{c}$	mean aerodynamic chord of basic wing, 4.462 in.
F	frontal area of fuselage, 7.07 sq in.
H	total pressure
M	Mach number
m	rate of internal mass flow
p	static pressure
q	dynamic pressure, $\frac{1}{2}\rho v^2$
R	Reynolds number, based on mean aerodynamic chord of basic model
$\rho$	mass density
S	basic wing area, 80.7 sq in.
t	wing section thickness expressed in percent c
v	local velocity parallel to surface and within boundary layer
$V_i$	local velocity parallel to surface at outer edges of boundary layer at the inlet measuring station
V	velocity
X	distance parallel to fuselage center line
Y	distance perpendicular to a plane through wing chord
$\alpha$	angle of attack

## Subscripts:

c	compressor-face station
i	inlet
o	free stream
S	bypass scoop
x	jet exit station

## MODEL CONFIGURATIONS

Basic model.- Photographs of the models are presented as figure 1. The basic model consisted of a wing of  $45^\circ$  quarter-chord sweep mounted with zero incidence in the midwing position on a fuselage of fineness ratio 6.7 (fig. 1(a)). The wing (table I) was composed of NACA 64A008 airfoil sections in the streamwise direction and had an aspect ratio of 4.032, a taper ratio of 0.6, no twist, and no dihedral. The basic fuselage was formed by rotating an NACA 652A015 airfoil about its chord line and is identical with the basic configuration of reference 1.

Inlet model.- Provision for installation of the inlet in the wing root was made by increasing the quarter-chord sweep of the basic wing in the inboard sections to  $60^\circ$  and by increasing the chord of the inboard sections resulting in a sweep of the inboard maximum thickness line of  $35^\circ$ . The thicknesses of the inboard wing sections were increased such that a spanwise cross section of the wing root taken at the line of maximum thickness formed a semiellipse which was symmetrical about the chord line. (See table I.) The resulting inboard sections were cut off along a line corresponding to the leading edge of the basic wing outboard of the inlet, and the inlet lips were faired around the semielliptical inlet shape from this new leading edge to the maximum thickness of the wing. The trailing-edge fillet resulting from the increase in chord increased the total wing area by 6.8 percent. As shown in table II, the inlet was made asymmetrical to provide a thick upper lip, desirable from low speed considerations (ref. 2) for obtaining a high maximum lift coefficient. A lower-lip stagger of  $30^\circ$  was also incorporated to improve the internal-flow characteristics at high angles of attack. This degree of stagger appeared to be a reasonable compromise between that required at low speeds and that shown to be excessive at high speeds (refs. 1 and 2). Pertinent dimensions of the inlet are found in table II. Elliptical ordinates were used for fairing the inner and outer inlet lips.

The projected frontal area of the inlets relative to the fuselage ( $A_1/F = 0.167$ ) was the same as for the triangular inlets tested in reference 1 which were designed to handle the air-flow requirements of a representative single-engine jet airplane assumed to be flying at an altitude of 35,000 feet, a Mach number of 1.0, and operating at an inlet mass-flow ratio of 0.8. The cross-sectional area of the internal duct was gradually reduced by 6.4 percent at the inlet rake measuring station. This reduction in cross-sectional area is due primarily to the curvature of the fuselage wall of the inlet duct.

Inasmuch as the two inlets were assumed to admit the air flow for one engine, the internal ducting for each inlet was designed to undergo a cross-sectional transition from a semielliptical shape at the inlet to

a semicircular shape and to merge at the assumed engine compressor face. The ratio of the area at the compressor measuring station to the area at the inlet measuring station was 1.115. The duct behind the compressor-face station was circular and led to an exit in the tail end of the fuselage. Four exit areas  $A_x/A_c$  of 1.0, 0.75, 0.50, and 0.25 were provided to vary the internal-flow rate, as shown in figure 2.

A boundary-layer bypass scoop which improved the total-pressure-recovery characteristics of the inlet was installed between the original inlet and fuselage wall for some of the tests. This installation was accomplished by removal of the fuselage surface immediately ahead of the inlet to a depth equal to that of the boundary-layer scoop and by refairing the fuselage contour and inlet lip-fuselage juncture. (See fig. 3.) The scoop-inlet-area ratio was  $A_s/A_1 \approx 0.11$ . The scoop flow was discharged through the lower surface of the wing near the maximum wing thickness station.

#### APPARATUS AND METHODS

Pressure measurements.- The pressure instrumentation used for the present tests was the same as that of reference 1 except for the distribution of total- and static-pressure tubes in the inlet rake (see fig. 4). As in reference 1 a dummy inlet rake identical with the inlet measuring rake was installed in the left duct in order to avoid flow asymmetry due to rake blockage when inlet measurements were made. The boundary-layer removal system tested was instrumented with one total- and one static-pressure tube in each duct.

Force and moment measurements.- In addition to measurements of lift and drag and lift and drag tares which were made in the same manner as in reference 1 (see fig. 5), pitching moments were measured in the present tests. In order to evaluate the effects of the inlet alone on pitching moment, an attempt was made to remove the effects of the jet exit. Inasmuch as the uniformity of the flow warranted the assumption that the momentum and base pressure force due to the jet act through the pitch center, the changes in pitching moment due to the jet exit result solely from elimination of the external pressure load on that part of the fuselage cut off to provide the exit and the changes in external pressure load on the fuselage afterbody due to the exit flow. The corrections made to compensate for the exit in the present tests were obtained by measuring the pitching moments of the basic model with the closed fuselage tail and with the fuselage cut off at stations corresponding to those of the inlet model. The difference in moment was algebraically added to the pitching moment of the inlet model. No correction has been made for the effect of the jet-exit flow on the pressures over the afterbody.

Tests. - Force and pressure tests were made separately in order to eliminate balance fouling by the model pressure tubing. Pressure-measurement tests were also made in two parts; the inlet rakes were removed when the compressor face pressures were measured so as not to measure losses caused by flow past the inlet rakes.

As was discussed in detail in reference 1, the absolute value of force data presented herein does not correspond to free air data due primarily to the large model-to-tunnel-size ratio. However, the more important aerodynamic effects of installation of the inlet in the wing root can be evaluated from the differences in forces between the inlet and basic configurations.

In testing the triangular air inlet (ref. 1), it was found that the model nose was in a longitudinal Mach number gradient for Mach numbers of 1.2 and greater. It was later found that a more uniform flow field at these Mach numbers could be obtained by shifting the model downstream. Consequently, for the present tests, data obtained at Mach numbers of 1.2 and greater were obtained with the model shifted downstream from its original position. This improvement in test technique resulted in a difference between the present basic model drags and those presented in reference 1 for Mach numbers of 1.20 and greater. An extension of the subsonic Mach number range and an increase in the number of test points for the present tests showed that the basic model drags of reference 1 were high at a Mach number of 0.80, the minimum test Mach number of reference 1. Additional differences in the two presentations of basic model drag data at angles of attack result from omitting a negligible strain-gage balance interaction in the reference paper. It should be noted, however, that the drag increment due to the inlet should be correct within the specified limits for all conditions of both papers except for the lowest Mach numbers of reference 1.

The method of presentation of data in the present report is identical with that of reference 1 throughout. Therefore, the incremental changes in force due to the installation of the inlet are comparable as are the total-pressure recoveries.

The range of test variables and the estimated maximum error in measured coefficients based on the scatter and repeatability of data points are given in the following table:



Variable	Range	Maximum estimated error
$M_0$	0.65 to 1.41	$\pm 0.01$
$R$	$5.5 \times 10^6$ to $7.4 \times 10^6$	(a)
$\alpha$	$0^\circ$ to $9.6^\circ$	$\pm 0.1^\circ$
$m_1/m_0$	0.3 to 0.86	$\pm 0.02$

<sup>a</sup>At any Mach number,  $R$  varied approximately  $\pm 2$  percent due to changes in stagnation temperature.

Measured coefficient	Estimated maximum error of coefficient
$C_D$	$\pm 0.001$
$C_L$	$\pm 0.01$
$C_m$	$\pm 0.003$
$\frac{H - p_0}{H_0 - p_0}$	$\pm 0.005$
$\frac{\bar{H}}{H_0}$ (weighted)	<sup>a</sup> $\pm 0.01$

<sup>a</sup>At the higher inlet mass-flow ratios ( $\frac{m_1}{m_0} \approx 0.8$ ), the maximum error is estimated to be  $\pm 0.005$ .

All tests were made in the Langley transonic blowdown tunnel. This tunnel is a slotted tunnel of octagonal cross section which measures 26 inches between flats. The pressure recording equipment is a rapid response type necessitated by the short running time of the tunnel (about 30 seconds). The test Mach number is a function of the losses through the tunnel and consequently changes with angle of attack for large test models such as the present one. The only variables which could be held constant throughout the present test were angle of attack and the corresponding Mach number for an initially set tunnel loss. The data presented as a function of a particular variable for a given set of conditions therefore necessarily result from cross plots of the initial data. Sufficient data were taken to insure proper fairing of the final curves.

## RESULTS AND DISCUSSION

## Internal Pressure Measurements

Flow at the inlet measuring station.- The same basic model nose contour was used for the present tests as that of reference 1. Measurements showed the flow ahead of the inlet was the same in both tests. At low angles of attack, the Mach number ahead of the inlet compression shock was essentially free stream.

The pressure surveys at the inlet measuring station were made primarily to determine the sources of loss in the inlet. The distribution and relative magnitude of the losses is clearly shown by use of isobars of impact pressure ratio as measured at the inlet measuring station (fig. 6). The principal loss observed was due to entrainment of fuselage boundary layer. This loss increased as the Mach number increased beyond the sonic value as a consequence, it is believed, of the interaction of the inlet compression shock with the fuselage boundary layer. For all inlet mass-flow ratios less than about 0.5 reversed or unstable flow was observed at the inlet measuring station for the entire test Mach number range (see, for example, fig. 7). As the Mach number increased, the inlet mass-flow ratio required for stable flow at the fuselage surface of the inlet increased. At a Mach number of 1.22, unstable flow in the entering boundary layer was observed for a mass-flow ratio of about 0.7 (see fig. 7,  $M_0 = 1.22$ ). This is believed to be largely due to the increasing losses from shock-boundary layer interaction with increasing Mach number.

Flow at the compressor face measuring station.- The loss due to the entering boundary layer ( $\alpha = 0^\circ$ ) is reflected in the decay of impact pressures along the fuselage wall of the duct (fig. 8). For practical inlet mass-flow ratios ( $\frac{m_1}{m_0} > 0.5$ ), the flow through both ducts is shown to be fairly symmetrical. For inlet mass-flow ratios less than about 0.5, flow asymmetry due to twin duct instability (ref. 3) was observed (fig. 8,  $\frac{m_1}{m_0} \approx 0.4$ ). From a plot of individual duct flow rate against total flow rate (fig. 9), it appears that the onset of instability occurs at  $\frac{m_1}{m_0} \approx 0.5$ .

The mean total-pressure recovery at the compressor face measuring station weighted with respect to mass-flow ratio is presented in figure 10 as a function of Mach number and mass-flow ratio for angles of attack of  $\alpha = 0^\circ$ ,  $4.2^\circ$ , and  $9.6^\circ$ . Also shown on this figure ( $\alpha = 0^\circ$ )

is the total-pressure recovery obtainable through a normal shock. At the design mass-flow ratio ( $m_1/m_0 = 0.8$ ), a maximum recovery ( $\bar{H}/H_0$ ) of 0.97 was obtained. The difference between the normal shock recovery and the measured recovery at a Mach number of 1.0 ( $\alpha = 0^\circ$ ) was about  $0.03H_0$  which could be attributed largely to entering boundary layer and internal duct losses. As the Mach number increased beyond the sonic value, there was a general decrease in total-pressure recovery. At an angle of attack of  $0^\circ$ , the recovery decreased to about  $0.90H_0$  at  $M_0 = 1.40$ . The difference between the measured total-pressure recovery and that obtainable through a normal shock at  $M_0 = 1.40$  was about  $0.06H_0$  indicating an increase in loss due to Mach number of about  $0.03H_0$  more than that expected due to normal shock losses. This increase in loss of recovery with increasing supersonic Mach number is believed to result from shock boundary-layer interaction as previously discussed. The relative magnitudes of the shock and boundary-layer losses, however, are not quantitatively known since measurements have shown that normal shock losses do not always exist in the outboard end of the inlet.

The effect of angle of attack was small for the design mass-flow-ratio condition. In general at the lower flow rates the total-pressure recovery increased with an increase in angle of attack in the supersonic Mach number range. This is believed to result primarily from boundary-layer thinning due to cross flow behind the inlet compression shock which moves forward with decreasing inlet flow rate and increasing angle of attack.

At Mach numbers greater than about 1.10, the recovery dropped off quite rapidly as the inlet mass-flow ratio was reduced (fig. 10(b)). This is generally to be expected since the boundary-layer growth and velocity profile are functions of the pressure gradient which the boundary layer must traverse. Reduction of the inlet flow makes this gradient more adverse. The increase in the rate of reduction in total-pressure recovery with decreasing inlet mass-flow ratios at Mach numbers greater than 1.10 results from the effect of the inlet compression shock interaction with the boundary layer immediately ahead of the inlet. At subsonic speeds, the variation in total-pressure recovery with inlet mass-flow ratio was small for conditions where duct flow symmetry existed.

#### Effect of Inlet Installation on External

##### Aerodynamic Characteristics

It was noted previously that, because of the large size of the model relative to the tunnel, the absolute force values measured are not comparable to free-air conditions, but that the incremental values due to the inlet installation should be correct within the estimated limits.

In order to present clearly the variation of the incremental force changes as a function of Mach number or other variables, the data are presented as the force coefficients of the basic configuration compared with the force coefficients of the basic configuration plus the incremental change due to the inlet installation. All coefficients are based on the wing area of the basic configuration. The increase in wing area of the inlet configuration due to the added area of the fillets was about 6.8 percent of the basic wing area.

Lift.- The variation of lift with angle of attack for various Mach numbers at inlet mass-flow ratios of 0.4 and 0.8 are presented in figure 11. The changes in lift due to the installation of the inlet were small. There was an apparent increase in lift at the higher angles of attack which is attributed to the increase in wing area resulting from the fillets.

Pitching moment.- The more significant changes in pitching moment due to installation of the inlet appeared generally as an increase in stability in a Mach number range near 1.0 (fig. 12). The incremental change of slope of the pitching moment curves due to the inlet was essentially zero at low subsonic speeds and again approached zero at the highest test Mach number ( $M_0 = 1.40$ ). Inasmuch as the maximum change of aerodynamic center due to Mach number occurs at the highest test Mach number, the detailed differences in stability between the basic and inlet configurations at the intermediate Mach numbers would be unimportant for an airplane designed to fly up to the maximum Mach number of these tests. There was a slight reduction in lift coefficient for pitch-up due to the inlet which appeared only in the Mach number range between  $M_0 = 0.975$  and  $M_0 = 1.10$ . At some Mach numbers, installation of the inlet actually increased the pitch-up lift coefficient slightly. The variation in pitching moment with inlet mass-flow ratio over the test speed range was generally within the accuracy of measurements for lift coefficients below that required for pitch-up.

Drag.- The external drag variation due to installation of the inlet is presented in figure 13 as a function of Mach number and inlet mass-flow ratio for angles of attack of  $\alpha = 0.1^\circ$ ,  $4.2^\circ$ , and  $9.6^\circ$ . At the two lower test angles, the drag increment due to the inlet was generally small. The maximum indicated increase in peak drag amounted to about  $\Delta C_{D_{ext}} = 0.005$  at  $\alpha = 4.2^\circ$  which is a much greater angle of attack than is required for level flight of a conventionally proportioned fighter-type airplane flying in the particular speed range. At higher supersonic speeds, the drag increase due to the inlet installation was again small. For the  $9.6^\circ$  angle-of-attack condition, a condition rarely encountered except during maneuvers, there appeared a drag reduction due to the inlet installation below a Mach number of 1.10. This reduction together with the increase in lift at this angle of attack (fig. 11) which appeared

generally over the same Mach number range indicates a possible reduction in the amount of wing-flow separation due to installation of the inlet. The change in peak drag was small and at higher supersonic speeds the drag increment due to the inlet approached zero.

The effect of inlet mass-flow ratio on the drag increment due to the inlet (fig. 13(b)) indicates that a minimum inlet drag would occur at the highest possible inlet mass-flow ratio. This fact, in conjunction with the indicated increase in total-pressure recovery with increasing inlet flow rate, points out the necessity of designing this type air inlet for as high a flow rate as possible, especially if the airplane on which it is to be used is designed to fly at supersonic speeds. A discussion of the inlet performance under these conditions is made in a later section.

#### Effect of Boundary-Layer Removal on Internal Pressure Recovery

Installation of the boundary-layer removal system (figs. 1(d) and 3) resulted in some improvement in internal total-pressure recovery even though the removal flow rate available was small. The average mass flow removed by the present scoop and bypass amounted to only about 3 percent of the inlet mass flow at  $m_1/m_0 = 0.8$ ,  $\alpha = 0^\circ$  to  $4.2^\circ$ , for the test Mach number range. The low boundary-layer removal rate results from a poor removal system exit design and is believed insufficient especially at supersonic speeds. The design of the present system was limited by the existing model construction.

The resulting gains in total-pressure recovery due to boundary-layer removal as measured at the compressor face station are indicated by the comparison of scoop-on recovery with scoop-off recovery in figure 14. Also shown ( $\alpha = 0^\circ$ ) is the recovery obtainable through a normal shock. For the design mass-flow ratio, a gain of about  $0.005H_0$  was indicated in the subsonic speed range. At supersonic speeds, the apparent gain was larger and amounted to about  $0.03H_0$  and  $0.02H_0$  at  $M_0 = 1.25$  and  $M_0 = 1.40$ , respectively. A comparison of the scoop-on recovery with the normal shock recovery shows that the subsonic loss was maintained up to a Mach number of about 1.25 ( $\alpha = 0^\circ$ ) as a result of boundary layer removal. Above this Mach number, the losses gradually increased indicating that the removal rate was insufficient. Larger gains in pressure recovery due to boundary-layer removal are indicated for inlet mass-flow ratios lower than the design value.

Inasmuch as the removal flow was discharged almost  $90^\circ$  to the axis of the model, the drag due to the boundary-layer removal was about proportional to the mass of air removed. Hence, any gain in performance

through gains in pressure recovery would be partially offset by drag increases with the present removal-system design. The relative gain in internal total-pressure recovery does indicate, however, the importance of a boundary-layer removal system for air inlets of this type, and it is believed that, with a proper system design, the overall performance of these inlets at transonic and low supersonic speeds could be made to approach that of a nose or forward underslung scoop inlet.

### Inlet Performance

Wing-root air inlets and fuselage scoop inlets operating at transonic speeds and mass-flow ratios less than unity in the presence of an initial fuselage boundary layer suffer certain penalties which are not experienced by the pitot-type inlets. These penalties result from the unfavorable effect of the presence of the inlet on the initial fuselage boundary layer and show up as a loss in internal total-pressure recovery or an increase in external drag or both. The relative magnitude of the two possible effects depends to a large extent on the size and velocity profile of the fuselage boundary layer and the inlet flow rate. Consequently, in evaluating an air inlet, a parameter should be used which accounts for both the drag and pressure recovery. The parameter used in the present evaluation is the ratio of the net propulsive thrust produced by an engine in conjunction with the inlet considered to that of the same engine with an ideal inlet; where the ideal inlet would be characterized by a zero drag increment and 100-percent total-pressure recovery.

Accordingly the losses in total-pressure recovery measured for the present inlet (with no boundary-layer removal scoop) have been converted to a loss of thrust  $\Delta C_T$  by the conversion curve in reference 4 and summed with the increment in drag due to the inlet installation  $\Delta C_D$ . This in turn was subtracted from the ideal thrust  $C_{T_{ideal}}$  of a turbo-jet engine matched with the inlet at a Mach number of 1.40, inlet mass-flow ratio of 0.8, and at an altitude of 35,000 feet and is presented as a fraction of the ideal thrust available for Mach numbers of 0.8 to 1.4 at angles of attack of  $0.1^\circ$  and  $4.2^\circ$  in figure 15. Also presented in figure 15 is the thrust schedule of the engine (in coefficient form based on basic wing area) and inlet mass-flow ratio schedule used for the calculation over the Mach number range considered. Most of the data used in the performance calculations were obtained by extrapolation of the drag and pressure-recovery data as a function of inlet mass-flow ratio. The angles of attack considered ( $\alpha = 0.1^\circ$  and  $4.2^\circ$ ) bracket the required angle of attack for level flight of a normally proportioned fighter-type airplane through the enclosed Mach number range.

The results of such calculations indicate that rather good performance can be obtained for  $0.1^\circ$  angle of attack up to a Mach number of

about 1.2 (maximum loss up to  $M_0 = 1.2 \approx 6$  percent  $C_{T_{ideal}}$ ). At the higher Mach numbers, the performance drops off as a result of loss in pressure recovery (maximum loss for entire test range  $\approx 10$  percent  $C_{T_{ideal}}$ ).

Increasing the angle of attack to  $4.2^\circ$  decreased the general level of performance of the inlet because of an increase in inlet drag. Comparison of the present inlet with the triangular inlet of reference 1 ( $\alpha = 0.4^\circ$ ) shows comparable performance for the two inlets except in the vicinity of a Mach number of 1.0 where installation of the triangular inlet resulted in a lower performance due to a larger inlet drag. At an angle of attack of about  $4^\circ$ , the semielliptical inlet had the better performance throughout the speed range largely because of lower inlet drags.

A comparison of the external drag increments and internal total-pressure recoveries of the triangular and semielliptical inlets are presented in figure 16 for an angle of attack of about  $4^\circ$  and a constant mass-flow ratio of 0.7 (the highest mass-flow ratio presented in ref. 1). This comparison at a constant mass-flow ratio is presented in contrast to the higher and varying mass-flow ratios used in figure 15. The semielliptical inlet is better from the drag standpoint in the transonic range. At supersonic speeds, the incremental drag due to the inlet installation is essentially the same in both cases. The pressure-recovery comparison shows the semielliptical inlet to be superior throughout the test speed range with the larger gains occurring at supersonic speeds.

Generally, it appears that relatively high performance can be expected for the properly designed and matched wing-root type inlet in the transonic speed range. Improvement in performance at supersonic speeds appears to depend largely on the development of a method to efficiently remove the effects of shock-boundary-layer interaction on the internal total-pressure recovery without severe cost in drag.

#### SUMMARY OF RESULTS

An investigation has been made in the Langley transonic blowdown tunnel at Mach numbers from 0.63 to 1.41 to determine the increments in lift, drag, and pitching moment due to the installation of a semielliptical-shaped air inlet in the root of a  $45^\circ$  sweptback wing and to study the internal-flow characteristics of the inlet. The test range of angle of attack and mass-flow ratio varied from  $0^\circ$  to  $9.6^\circ$  and 0.3 to 0.86, respectively. The more important results are summarized as follows:

1. At a test inlet mass-flow ratio of 0.80 (angles of attack of  $0^\circ$  and  $4.2^\circ$ ), a maximum total-pressure recovery of 97 percent was obtained for Mach numbers up to 1.0. The total-pressure recovery decreased with

increasing supersonic Mach number to a value of about 90 percent at a Mach number of 1.40. The total-pressure recovery increased rapidly with increasing mass-flow ratio for Mach numbers above about 1.10.

2. The principal loss observed in the internal flow resulted from entrainment of the initial fuselage boundary layer by the inlet. This loss is believed to be magnified considerably by shock boundary-layer interaction.

3. Removal of only about 3 percent of the inlet air through a boundary-layer removal scoop increased the subsonic total-pressure recovery 0.5 percent and the total-pressure recovery at Mach numbers of 1.25 and 1.40, 3.5 percent and 2.0 percent, respectively, for angles of attack of  $0^\circ$  and  $4.2^\circ$ .

4. The incremental changes in external aerodynamic force characteristics due to the installation of the inlet were generally small. A maximum increase in drag coefficient of about 0.005 occurred at an angle of attack of about  $4^\circ$ . The primary effect of the inlet installation on the pitching moments was an increase in longitudinal stability in a Mach number range near 1.0.

5. At small positive lift coefficients ( $0^\circ$  angle of attack), the present inlet and the triangular inlet of NACA RM L52H08a had comparable performance for the design case considered. At an angle of attack of about  $4^\circ$ , the semielliptical-inlet performance was better primarily because of a lower inlet drag increment.

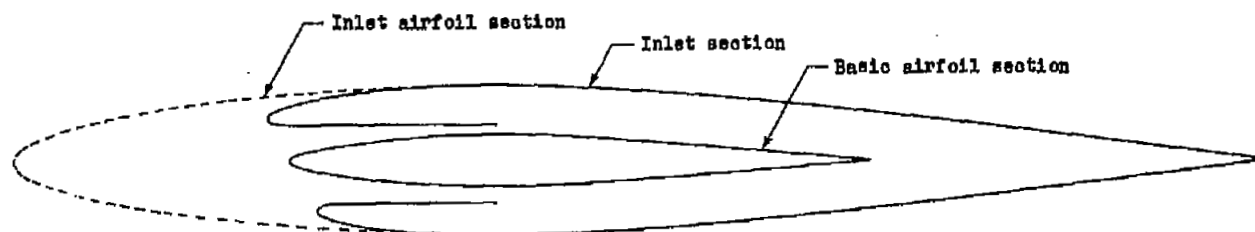
Langley Aeronautical Laboratory,  
National Advisory Committee for Aeronautics,  
Langley Field, Va., October 9, 1953.



## REFERENCES

1. Howell, Robert R., and Keith, Arvid L., Jr.: An Investigation at Transonic Speeds of the Aerodynamic Characteristics of an Air Inlet Installed in the Root of a  $45^\circ$  Sweptback Wing. NACA RM L52H08a, 1952.
2. Keith, Arvid L., Jr., and Schiff, Jack: Low Speed Wind-Tunnel Investigation of a Triangular Sweptback Air Inlet in the Root of a  $45^\circ$  Sweptback Wing. NACA RM L50I01, 1950.
3. Martin, Norman J., and Holzhausel, Curt A.: Analysis of Factors Influencing the Stability Characteristics of Symmetrical Twin-Intake Air-Induction Systems. NACA TN 2049, 1950.
4. Schueller, Carl F., and Esenwein, Fred T.: Analytical and Experimental Investigation of Inlet-Engine Matching for Turbojet-Powered Aircraft at Mach Numbers up to 2.0. NACA RM E51K20, 1952.

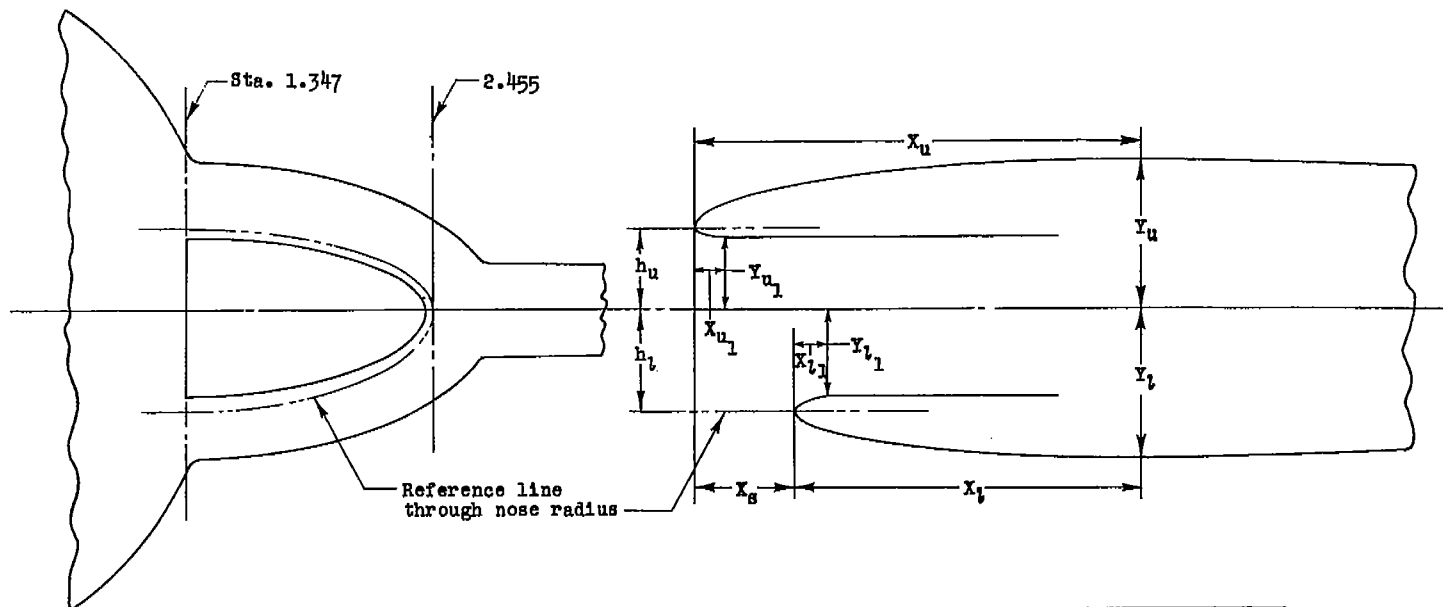
TABLE I- DESIGN DIMENSIONS OF BASIC AND DUCTED WING



Semispan wing station (in.)	Basic wing			Ducted wing				
	c (in.)	t (percent c)	$\alpha/4$ sweep	Total c (in.) (a)	t (percent total c)	$\alpha/4$ sweep	Inlet c (in.)	t (percent inlet c)
0	5.587	8	45°					
1.347	5.250	8	45°	11.250	11.11	60°	8.777	14.24
1.500	5.212	8	45°	10.522	11.80	60°	8.334	14.90
1.750	5.150	8	45°	9.331	12.83	60°	7.608	15.75
2.000	5.087	8	45°	8.141	13.59	60°	6.883	16.07
2.250	5.025	8	45°	6.951	13.74	60°	6.157	15.53
<sup>b</sup> 2.455	4.973	8	45°	5.976	12.78	60°	5.562	13.74
2.677	4.918	8	45°	4.918	8.00	60°	5.432	8.00
3.000	4.837	8	45°	4.837	8.00	45°	4.837	8.00
3.284	4.766	8	45°	4.766	8.00	45°	4.766	8.00
3.347	4.750	8	45°	4.750	8.00	45°	4.750	8.00
4.500	4.462	8	45°	4.462	8.00	45°	4.462	8.00
9.000	3.337	8	45°	3.337	8.00	45°	3.337	8.00

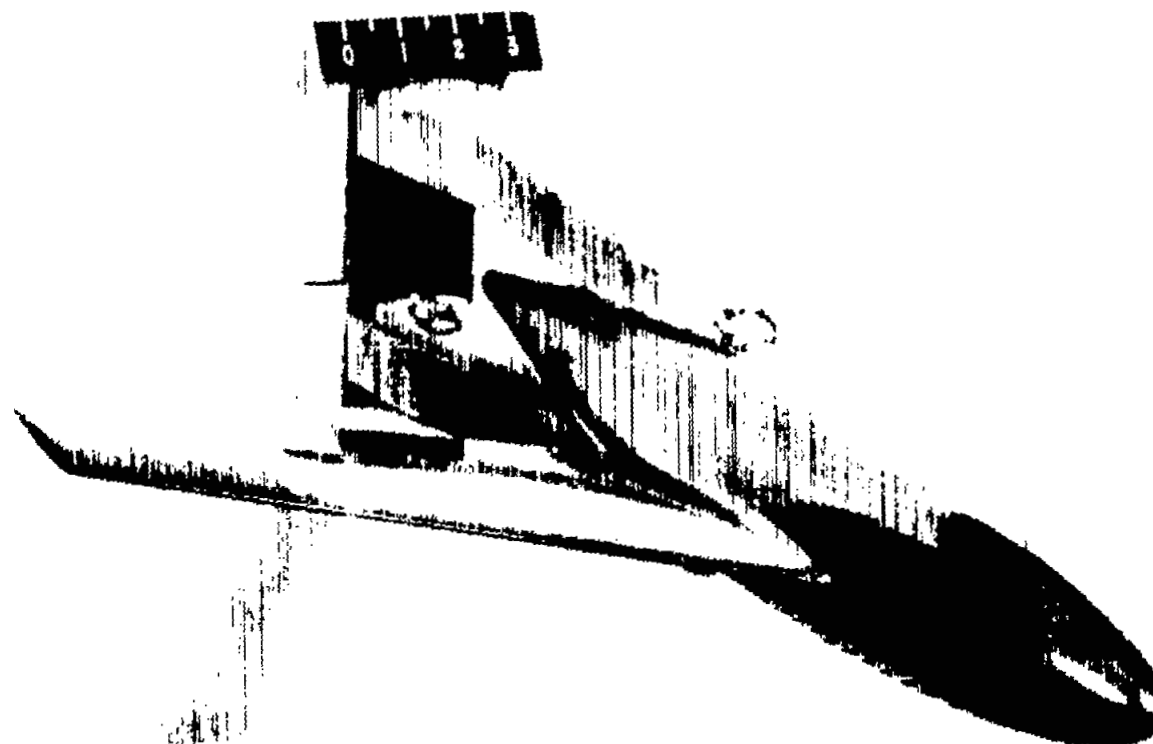
(a) Chord before installation of inlet  
 (b) Outboard end of inlet

TABLE II- DESIGN DIMENSIONS OF WING ROOT INLET CONFIGURATION  
( All dimensions in inches)



Wing station	External surfaces (a)							Internal surfaces (a)			
	$h_u$	$X_u$	$Y_u$	$X_s$	$h_l$	$X_l$	$Y_l$	$X_{u1}$	$Y_{u1}$	$X_{l1}$	$Y_{l1}$
1.347	0.338	1.998	0.625	0.442	0.428	1.556	0.626	0.125	0.300	0.185	0.366
1.500	.334	2.003	.621	.437	.423	1.567	.621	.125	.296	.185	.361
1.750	.314	2.004	.599	.411	.398	1.593	.599	.125	.278	.185	.338
2.000	.273	1.991	.553	.357	.345	1.635	.553	.125	.238	.185	.289
2.250	.195	1.960	.478	.256	.248	1.705	.478	.125	.161	.185	.196

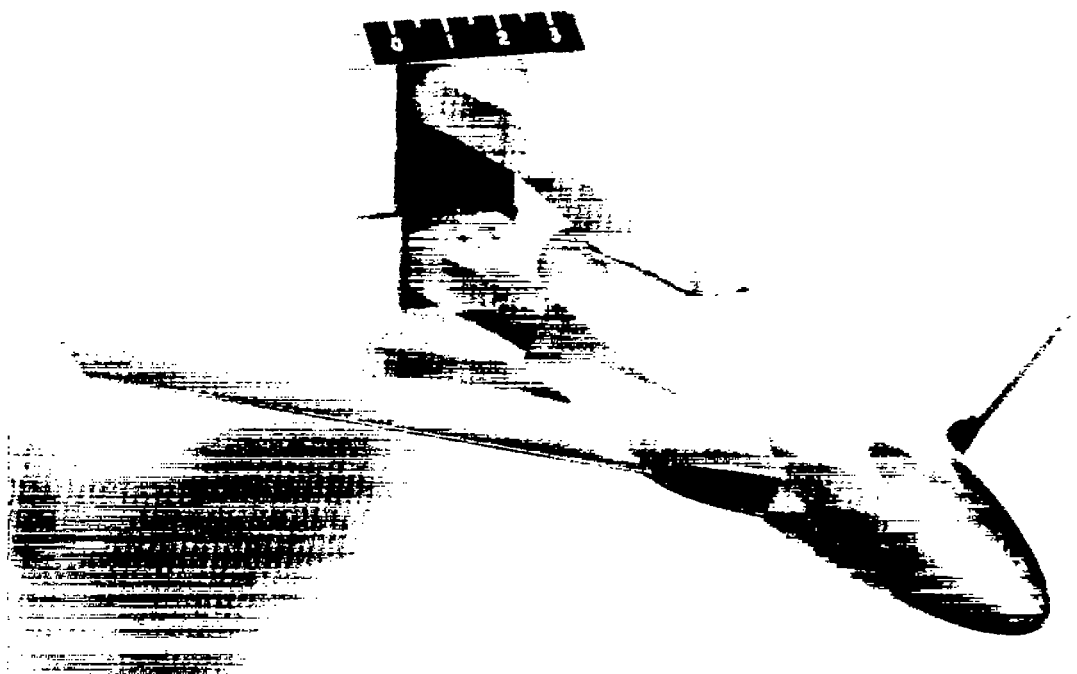
(a) External and internal nose shapes determined from elliptical ordinates



(a) Basic model; three-quarter view from above.

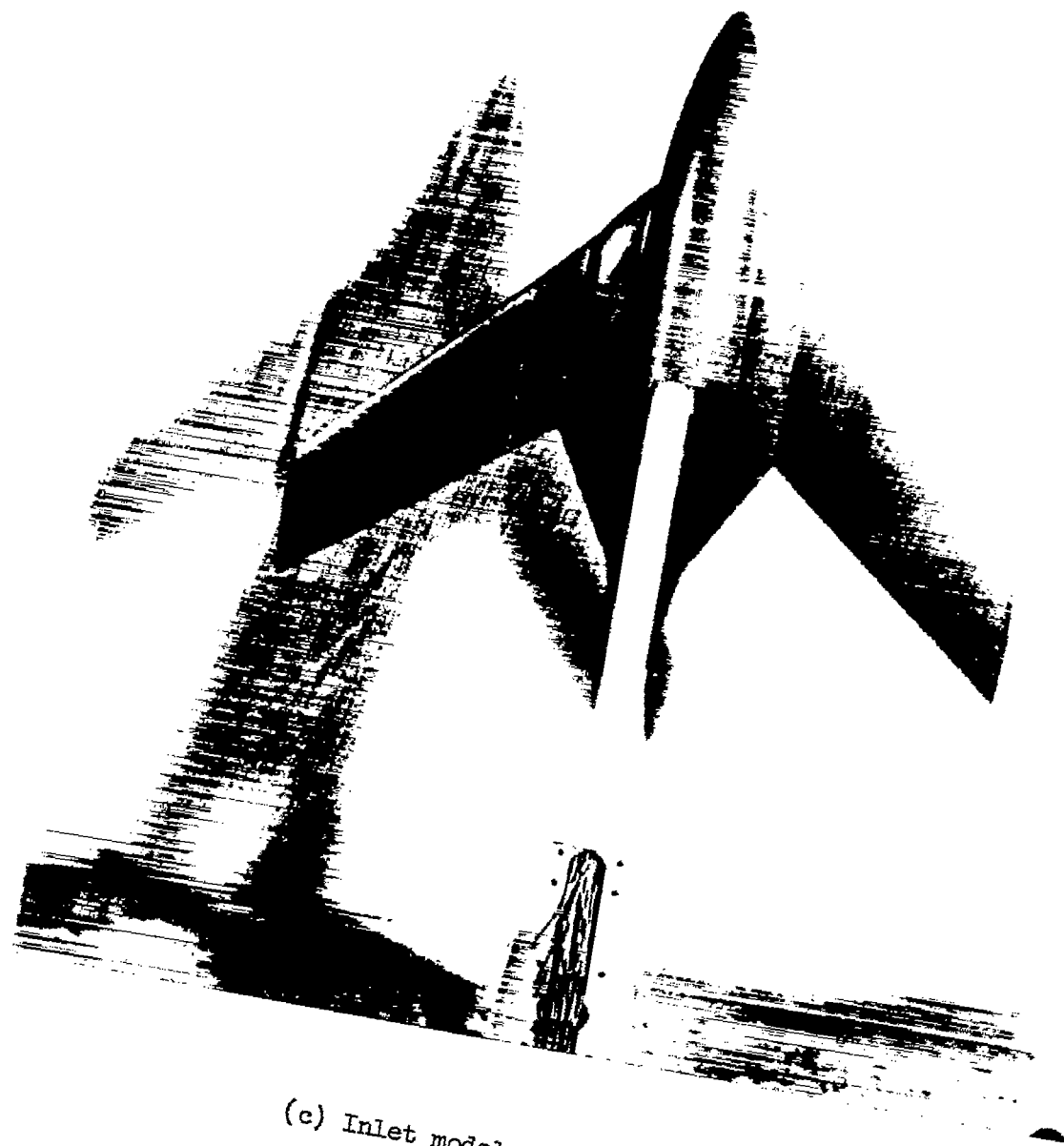
L-78977

Figure 1.- Photographs of the basic and inlet models.



(b) Inlet model; three-quarter view from above. L-78974

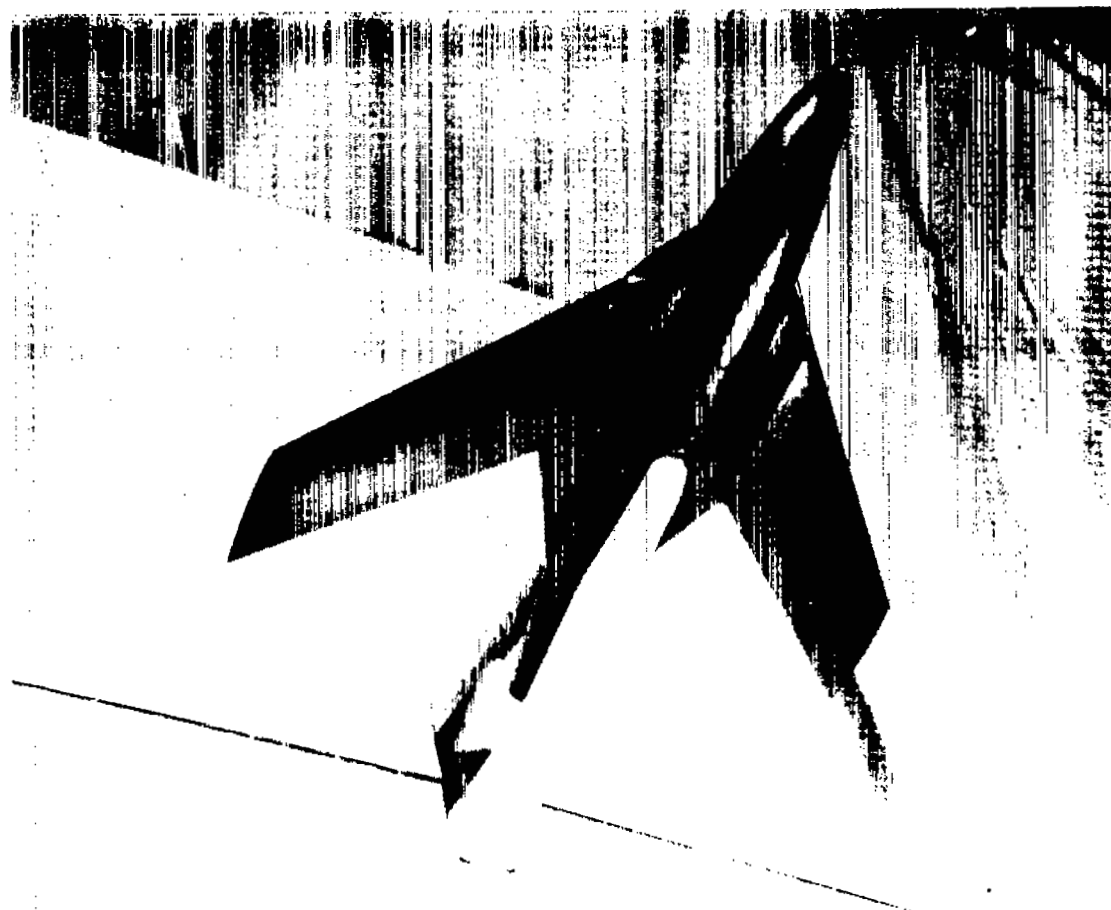
Figure 1.- Continued.



(c) Inlet model; plan view.

Figure 1.- Continued.

L-76796



L-76793

(d) Inlet model with boundary-layer bypass scoop;  
three-quarter view from below.

Figure 1.- Concluded.

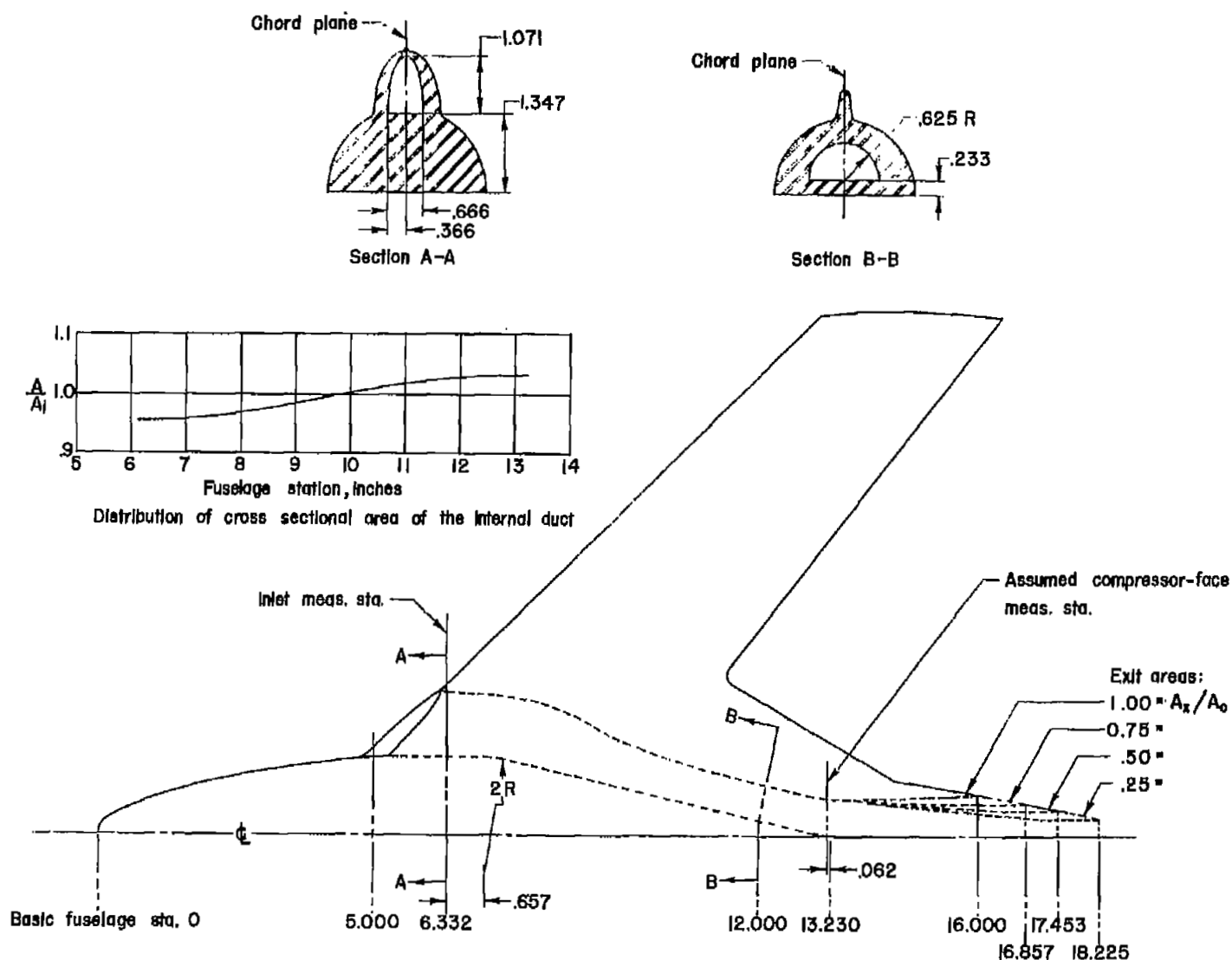


Figure 2.- Plan view of inlet model showing the details of internal ducting and exit configuration. All dimensions are in inches.



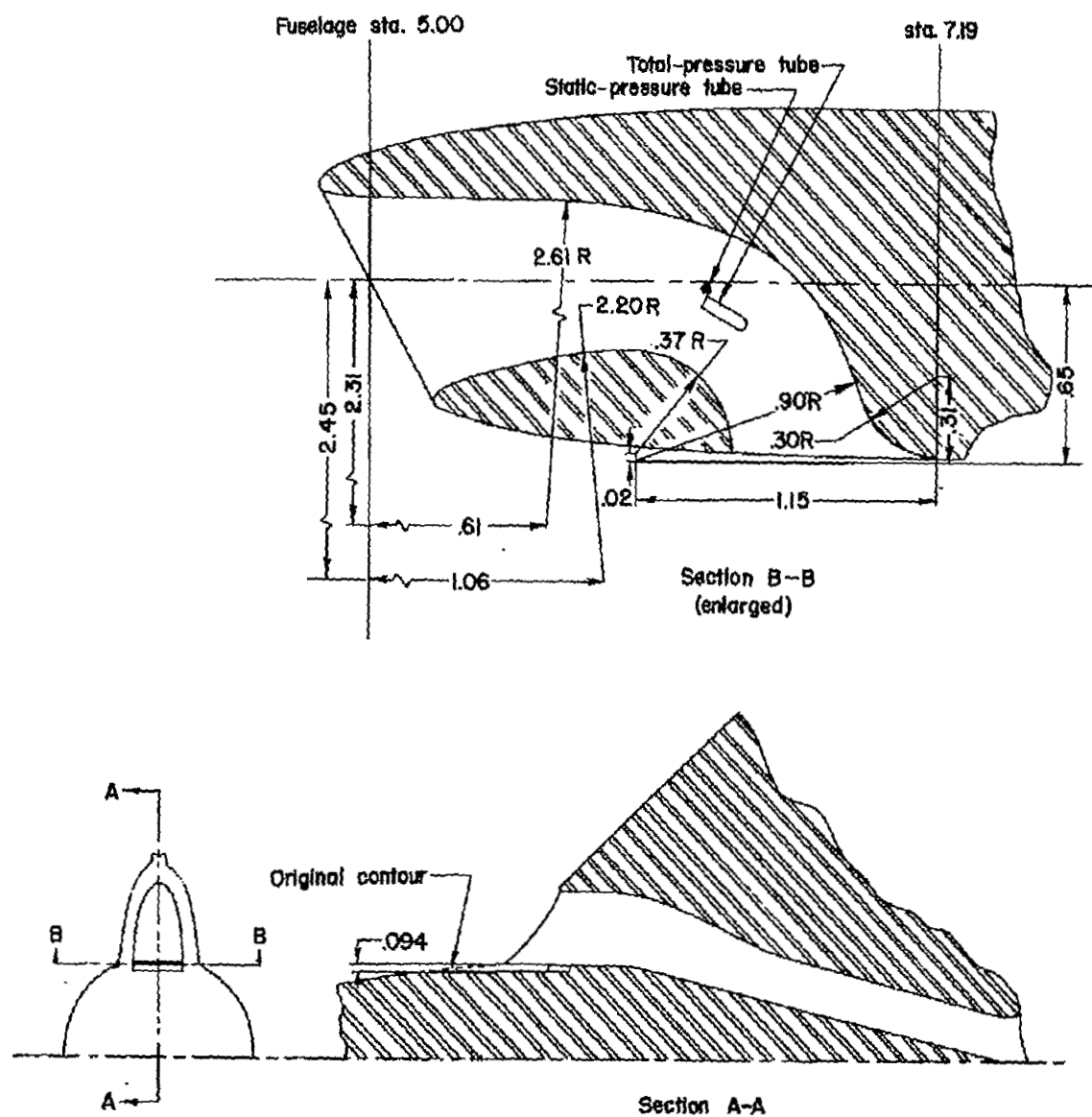


Figure 3.- Details of boundary-layer bypass scoop. All dimensions are in inches.

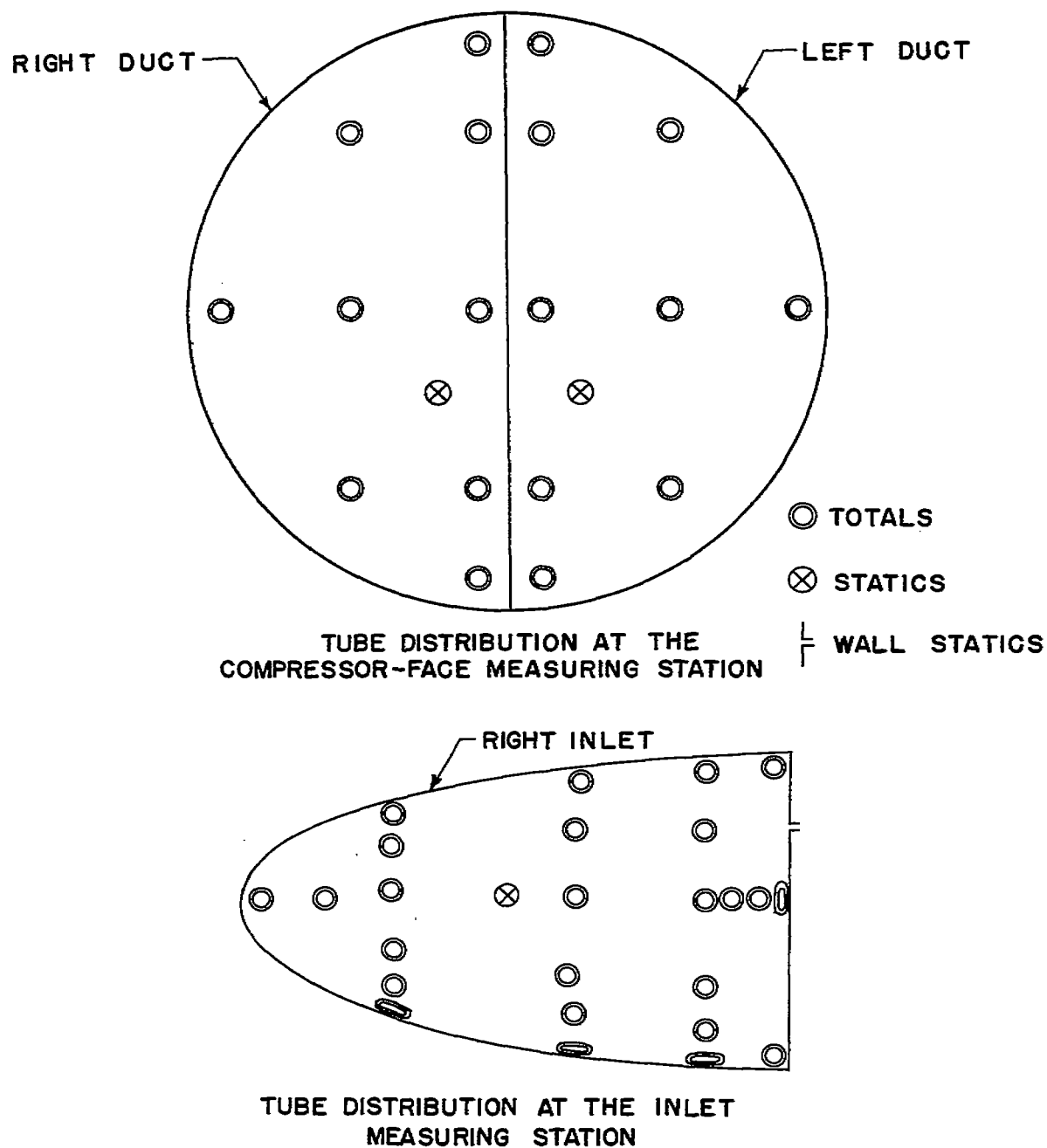
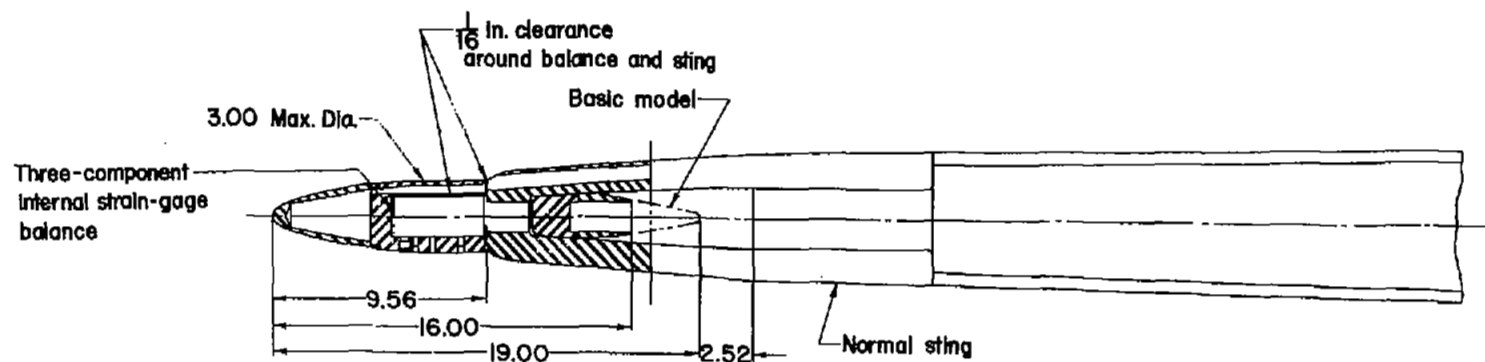


Figure 4.- Total- and static-pressure tube distributions at the inlet and compressor-face measuring stations.



Section A-A

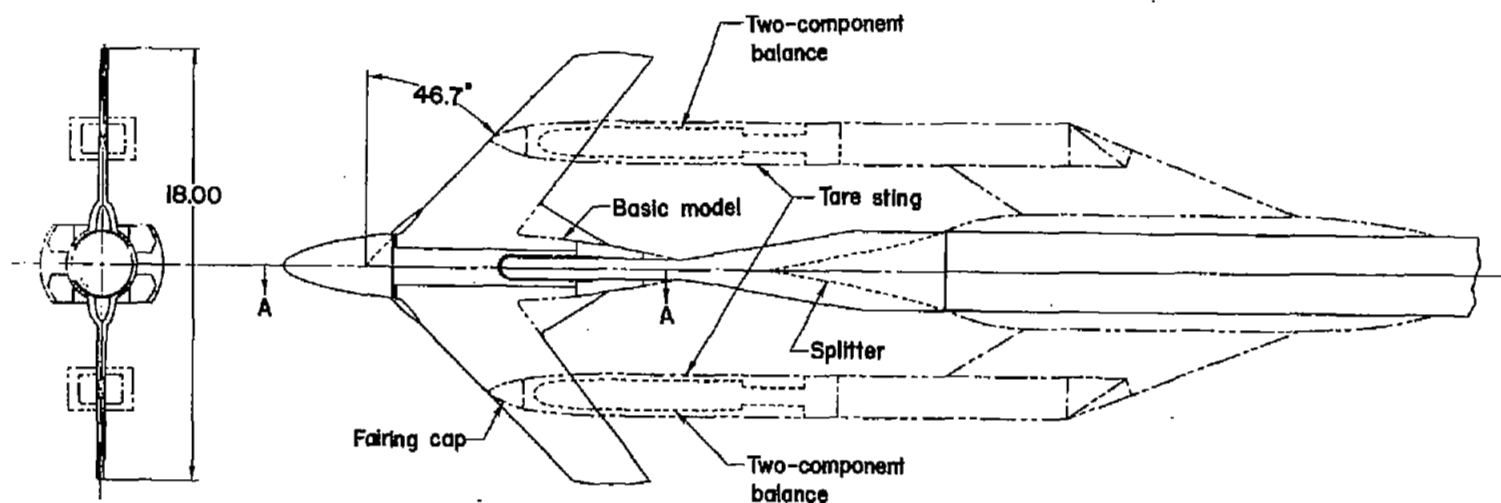


Figure 5.- General arrangement of models and model supports. All dimensions are in inches.

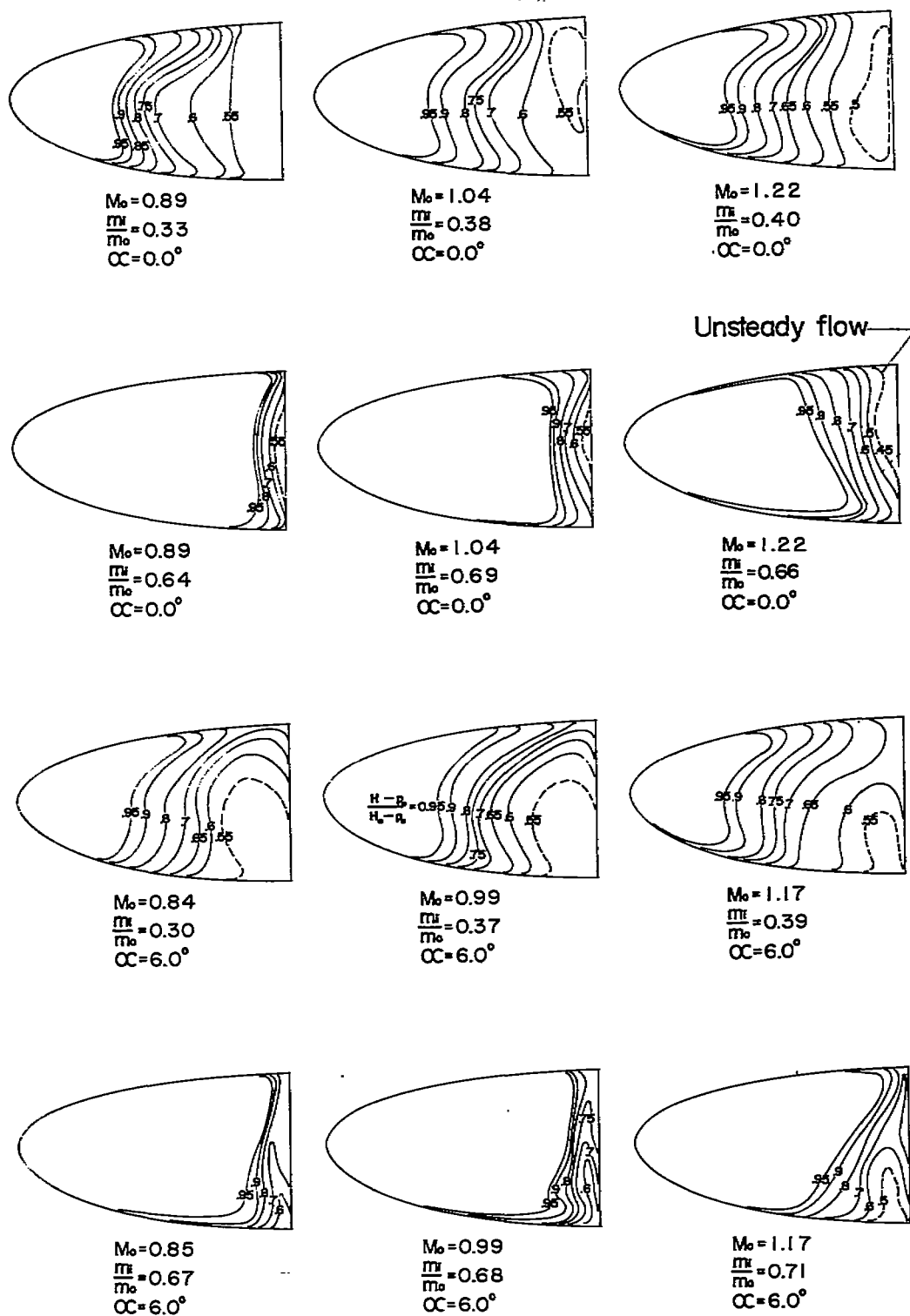


Figure 6.- Contours of impact pressure ratio at the inlet measuring station.

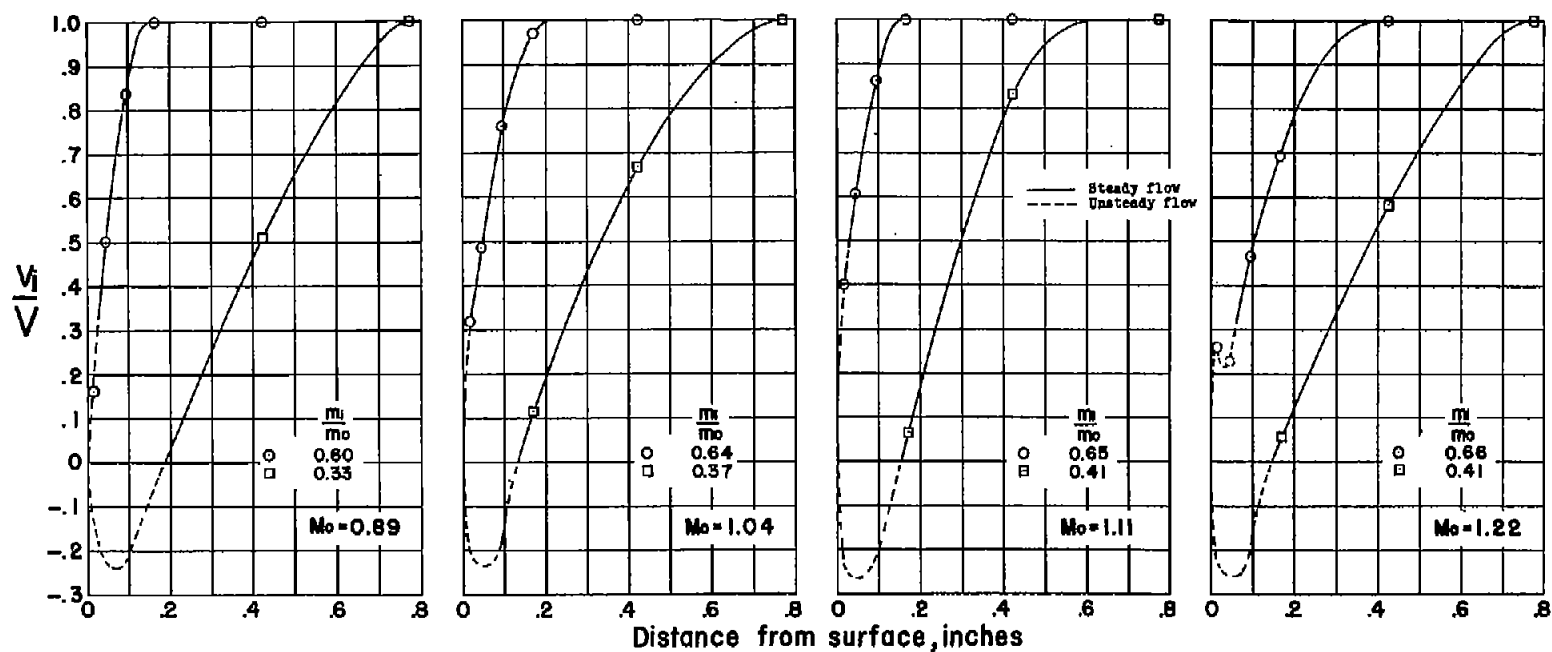


Figure 7.- Velocity profiles in the fuselage boundary layer at the inlet measuring station.  $\alpha = 0^\circ$ ; no boundary-layer scoop.

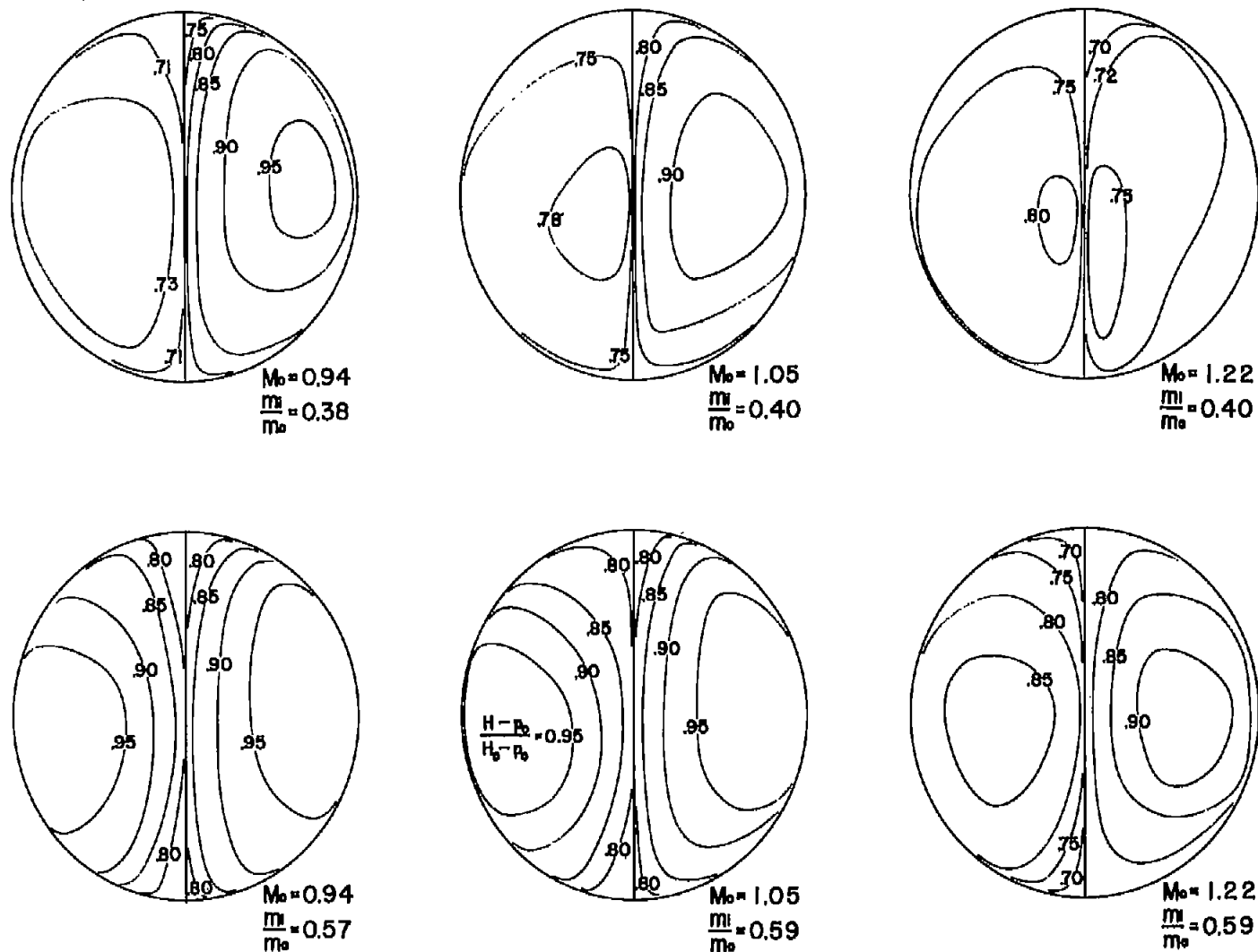


Figure 8.- Contours of impact pressure ratio at the compressor-face measuring station.  $\alpha = 0^\circ$ .

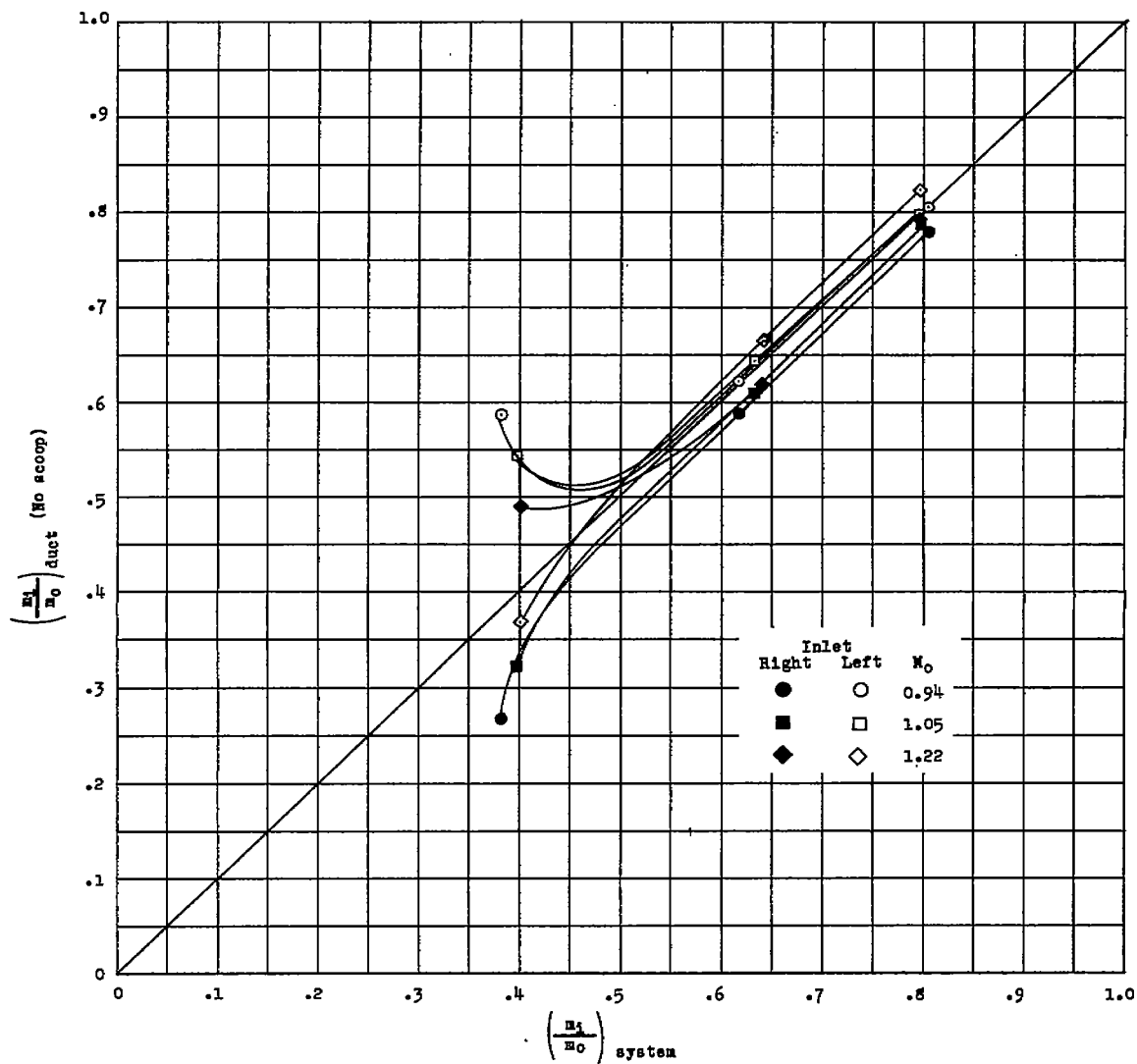
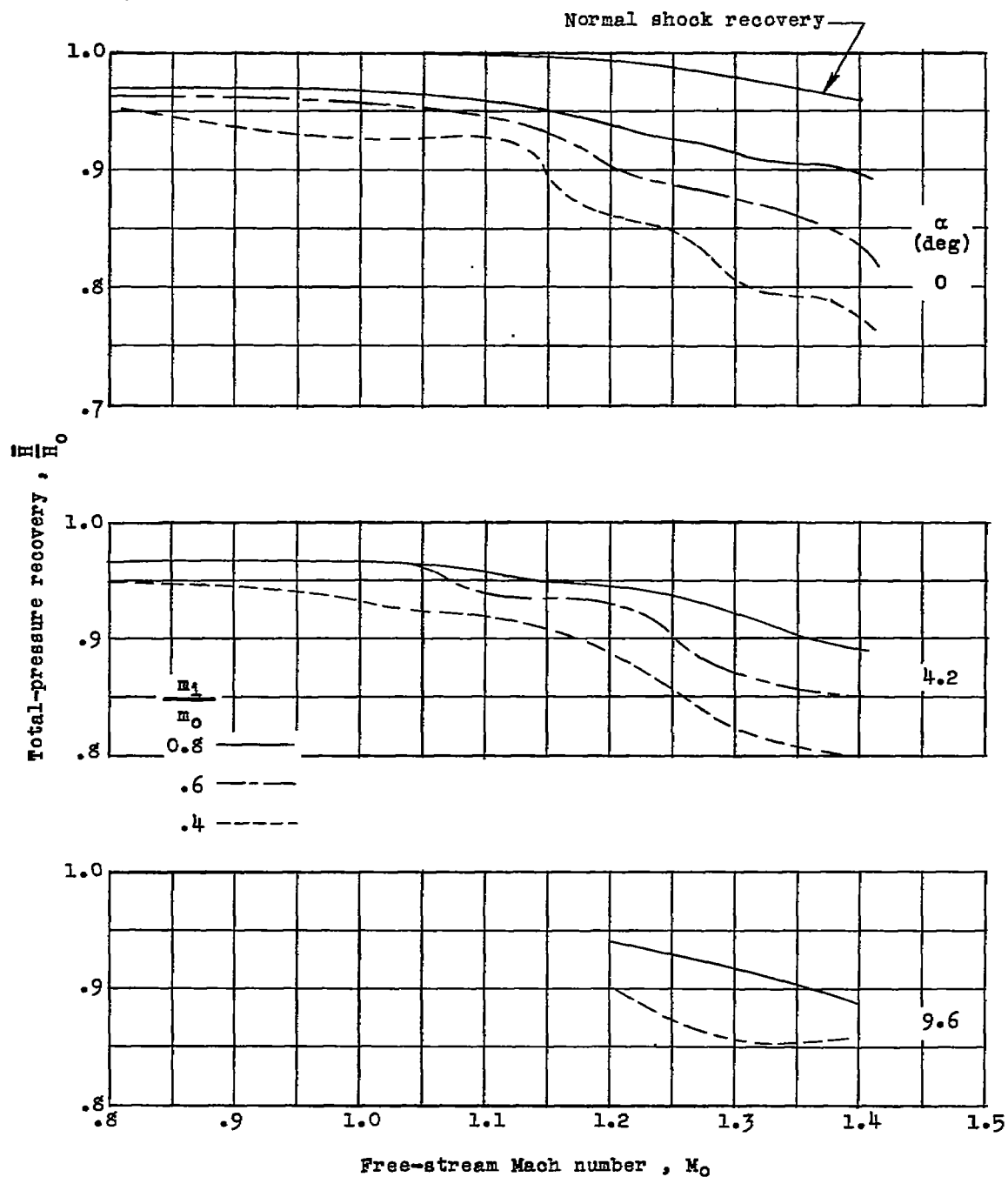


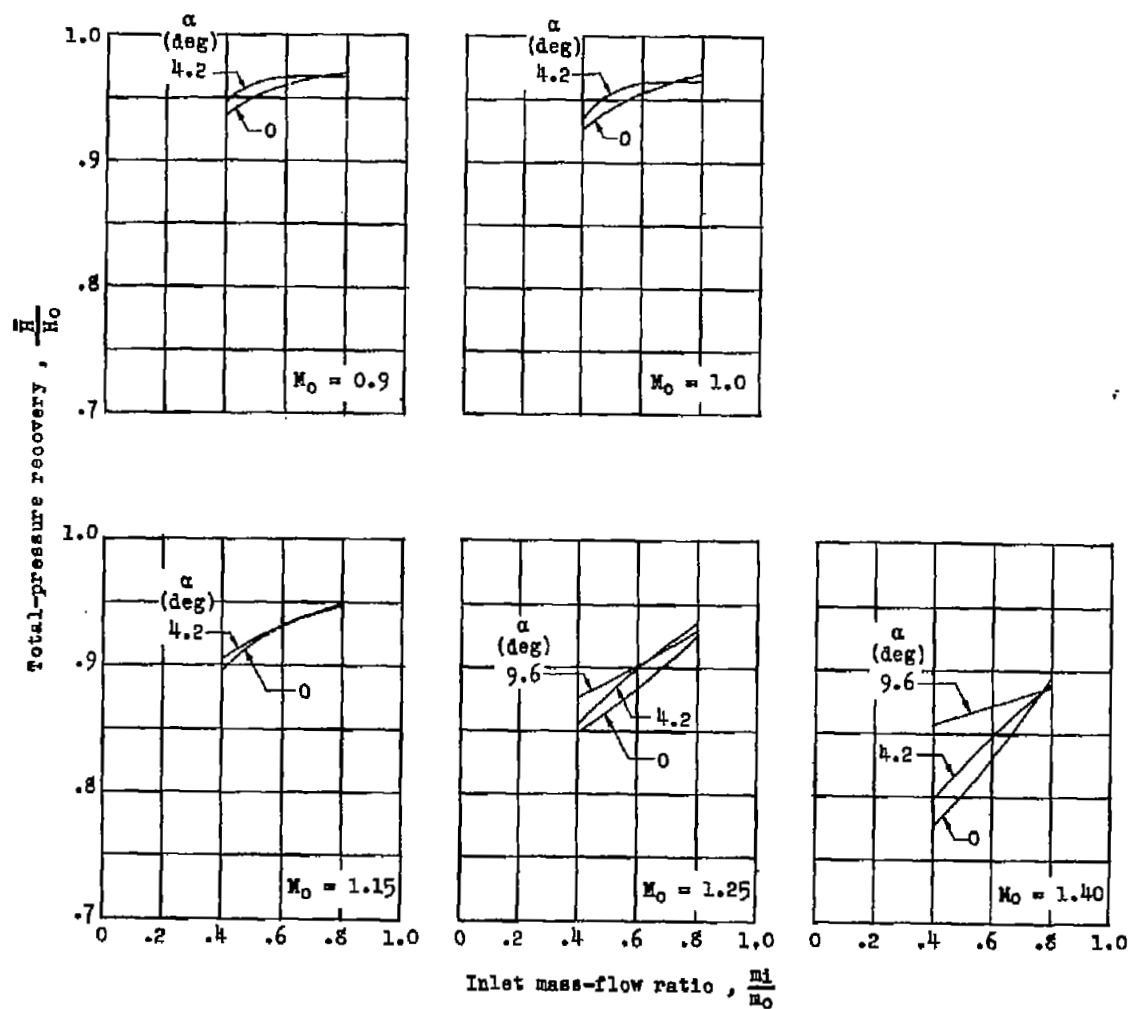
Figure 9.- Variation of individual duct flow rate with total internal flow rate.  $\alpha = 0^\circ$ .



(a) Effect of Mach number and angle of attack.

Figure 10.- Effect of variation of Mach number, angle of attack, and mass-flow ratio on the weighted total-pressure recovery at the compressor-face measuring station.





(b) Effect of mass-flow ratio.

Figure 10.- Concluded.

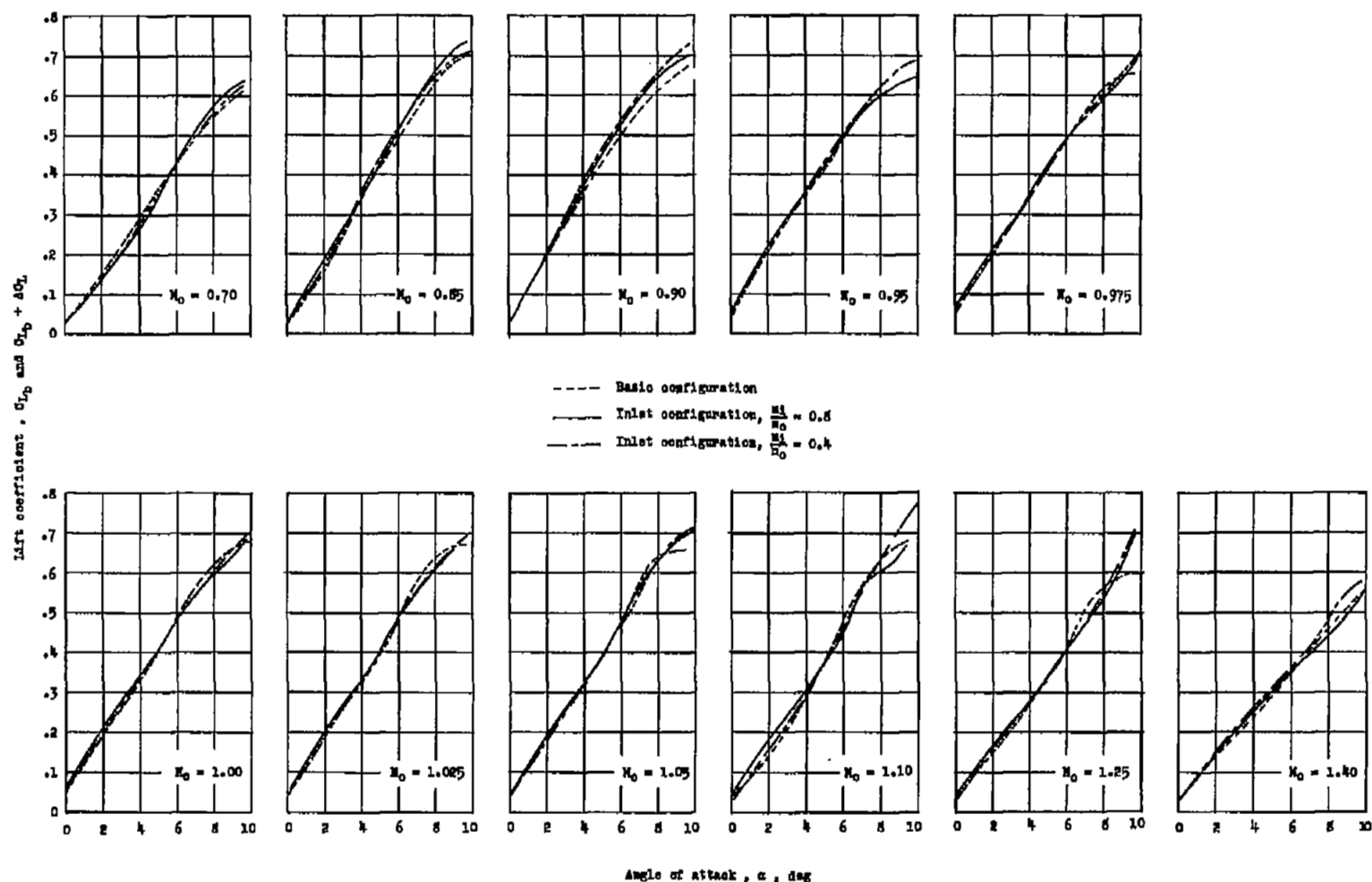


Figure 11.- Effect of angle of attack and inlet mass-flow ratio on the lift coefficient for Mach numbers covering the test range.

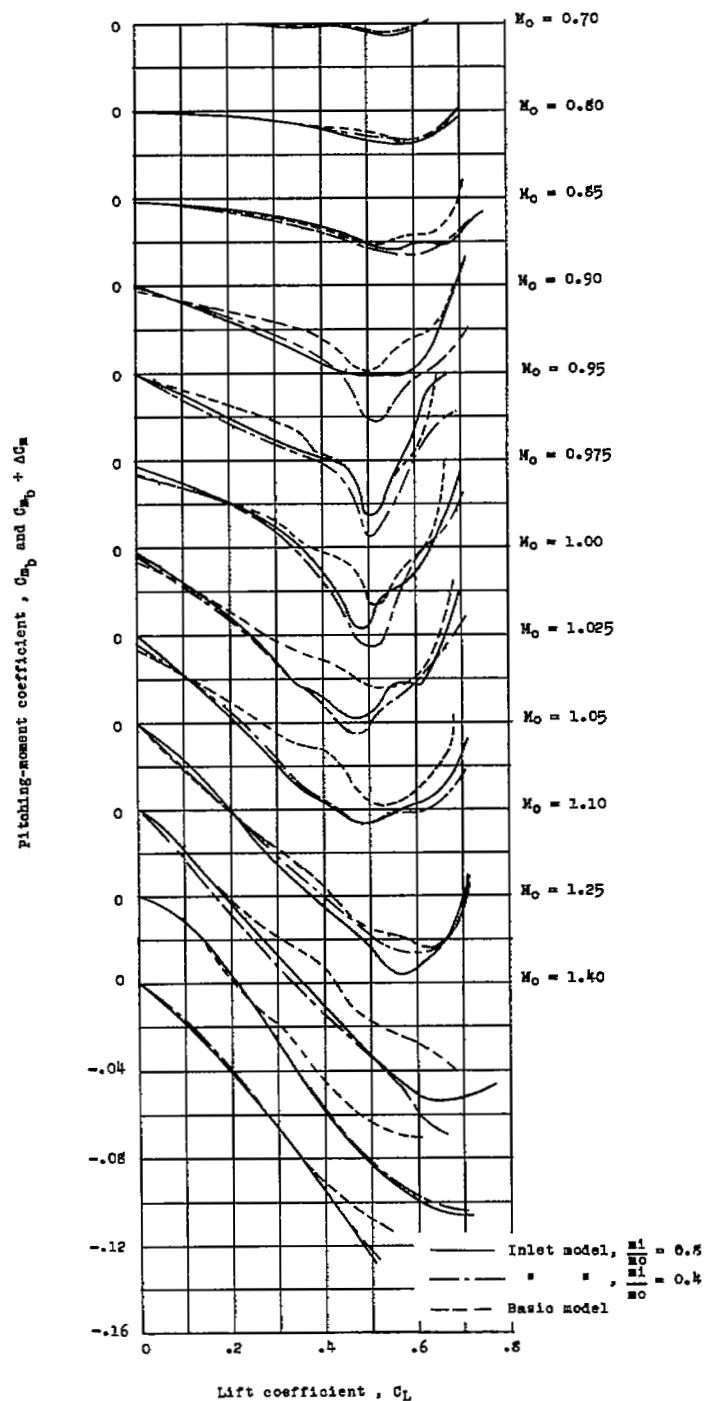
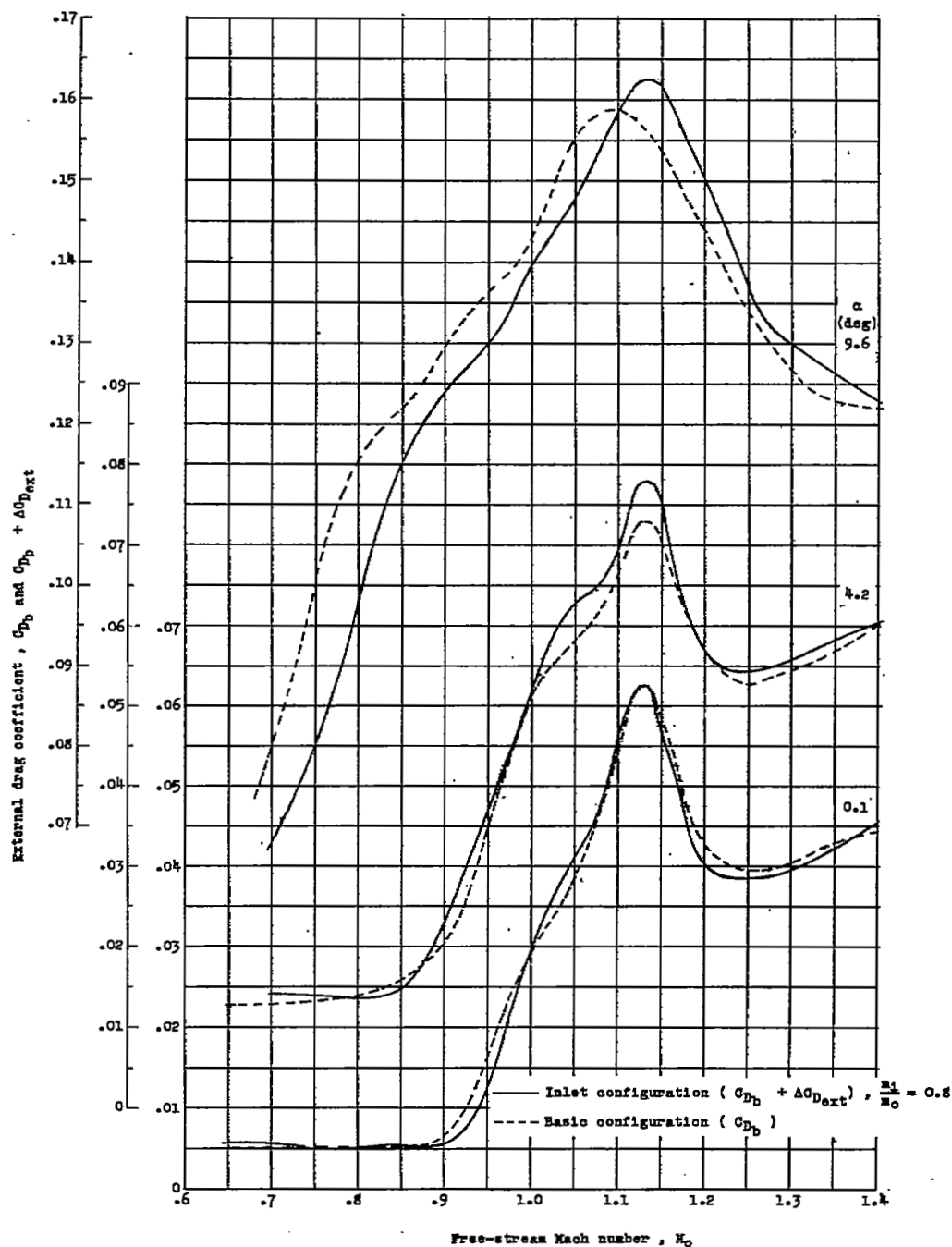
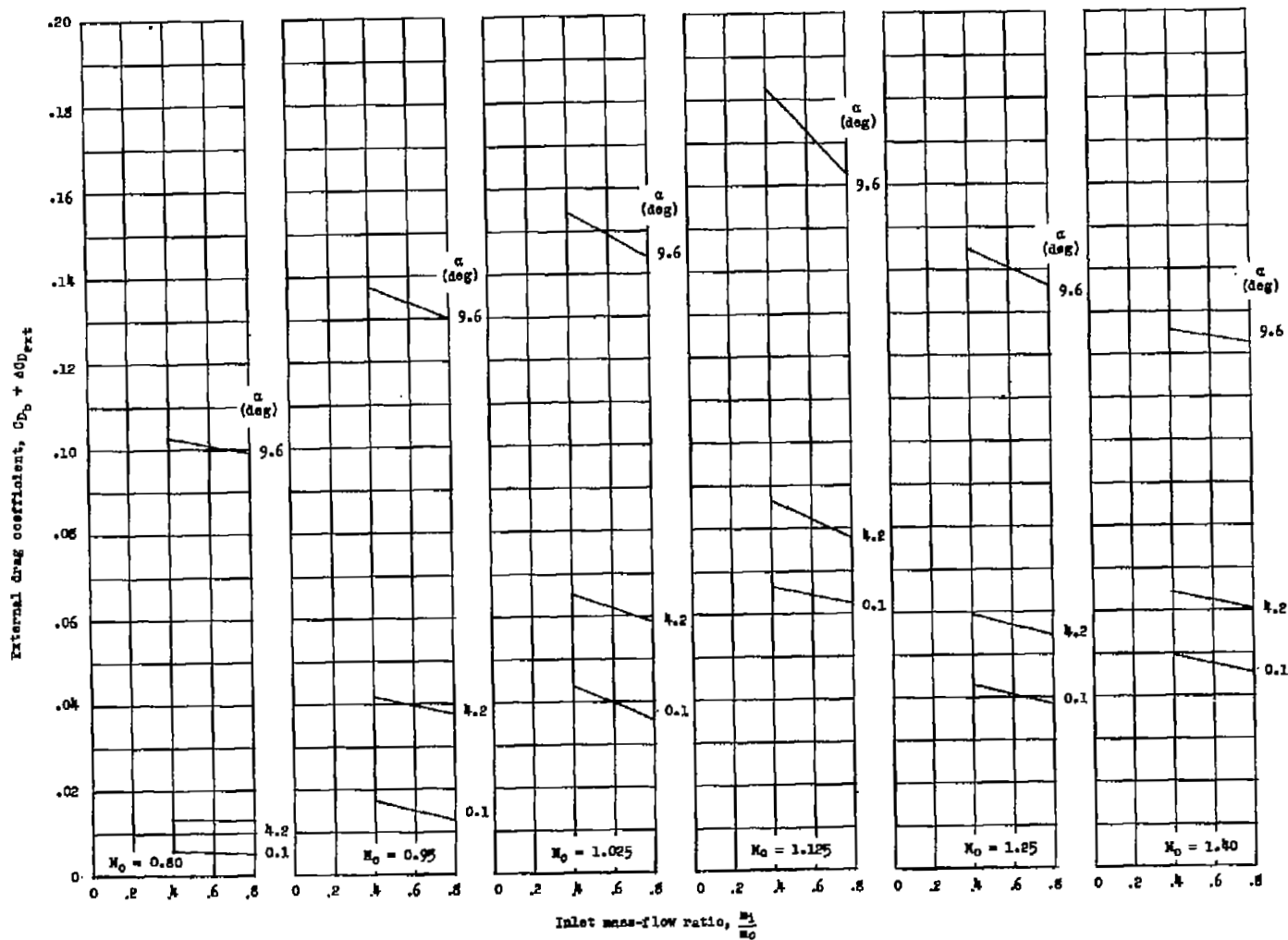


Figure 12.- A comparison of the variation of pitching moment with lift coefficient for Mach numbers covering the test range for the basic and inlet configuration.



(a) Effect of Mach number.

Figure 13.- Effect of variation of Mach number, angle of attack, and inlet mass-flow ratio on external drag.



(b) Effect of mass-flow ratio.

Figure 13.- Concluded.

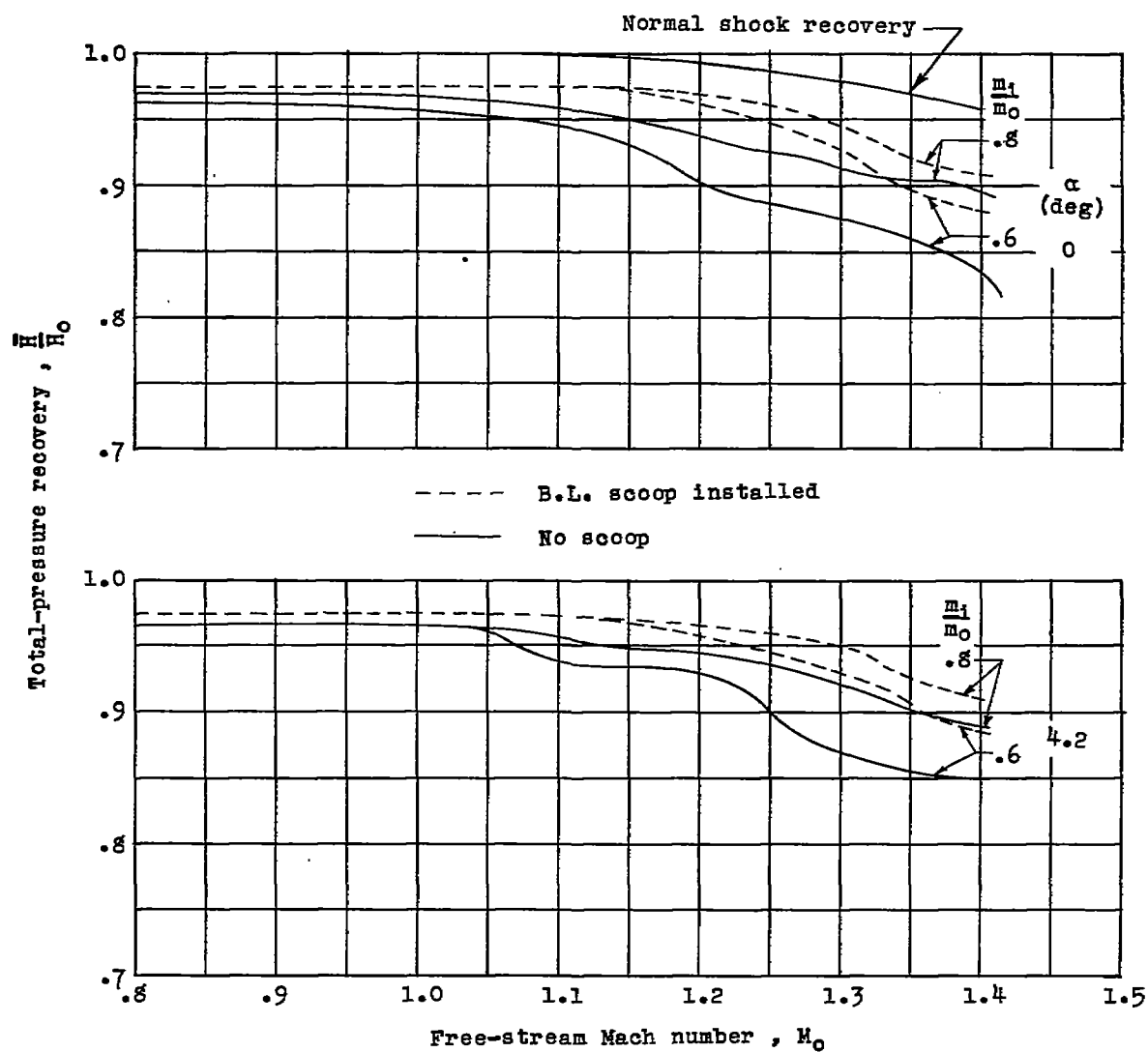


Figure 14.- Effects of boundary-layer removal on internal total-pressure recovery.

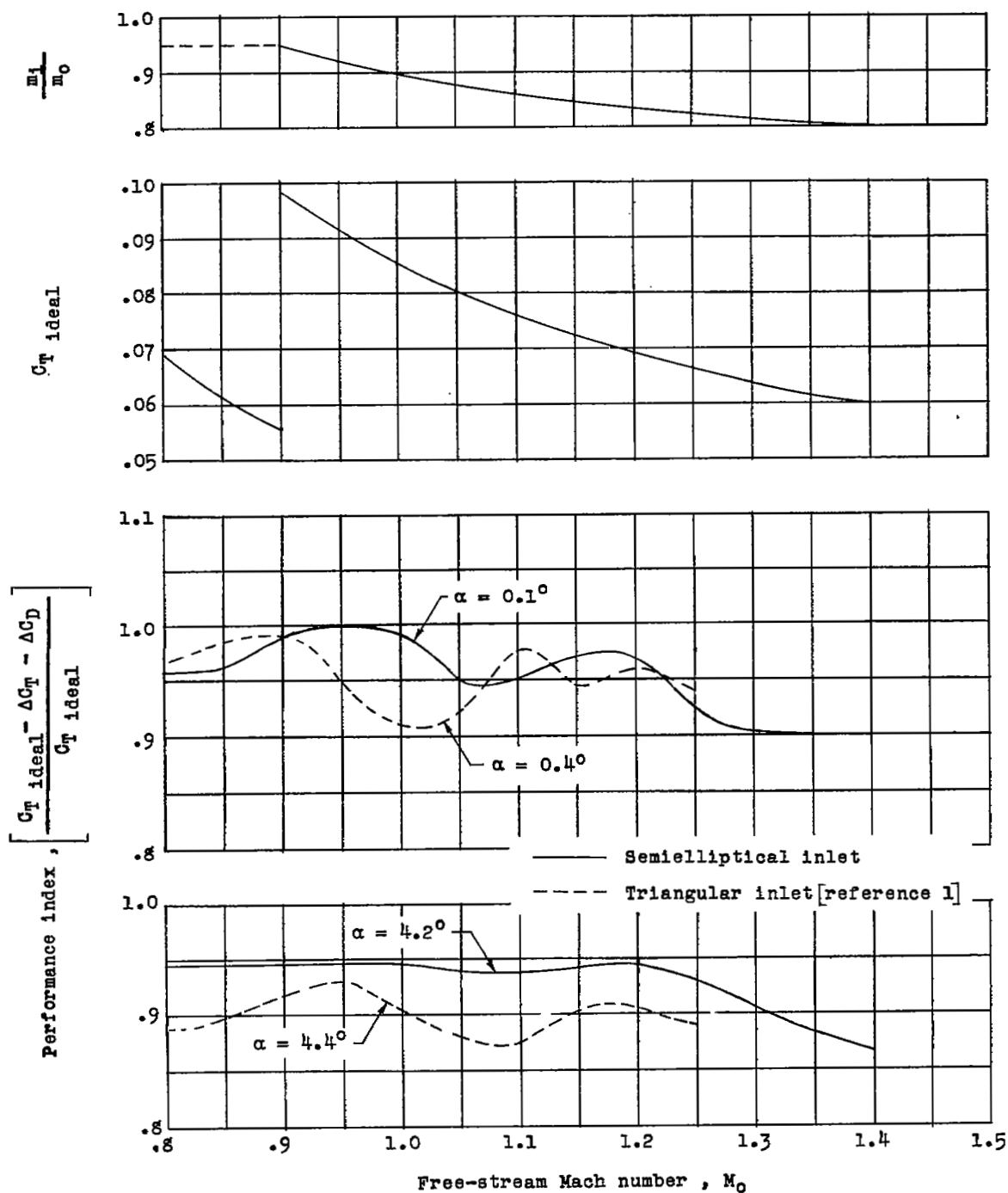


Figure 15.- Variation of inlet performance with Mach number for a chosen schedule of thrust and inlet mass-flow ratio for angles of attack of  $0.1^\circ$  and  $4.2^\circ$ .

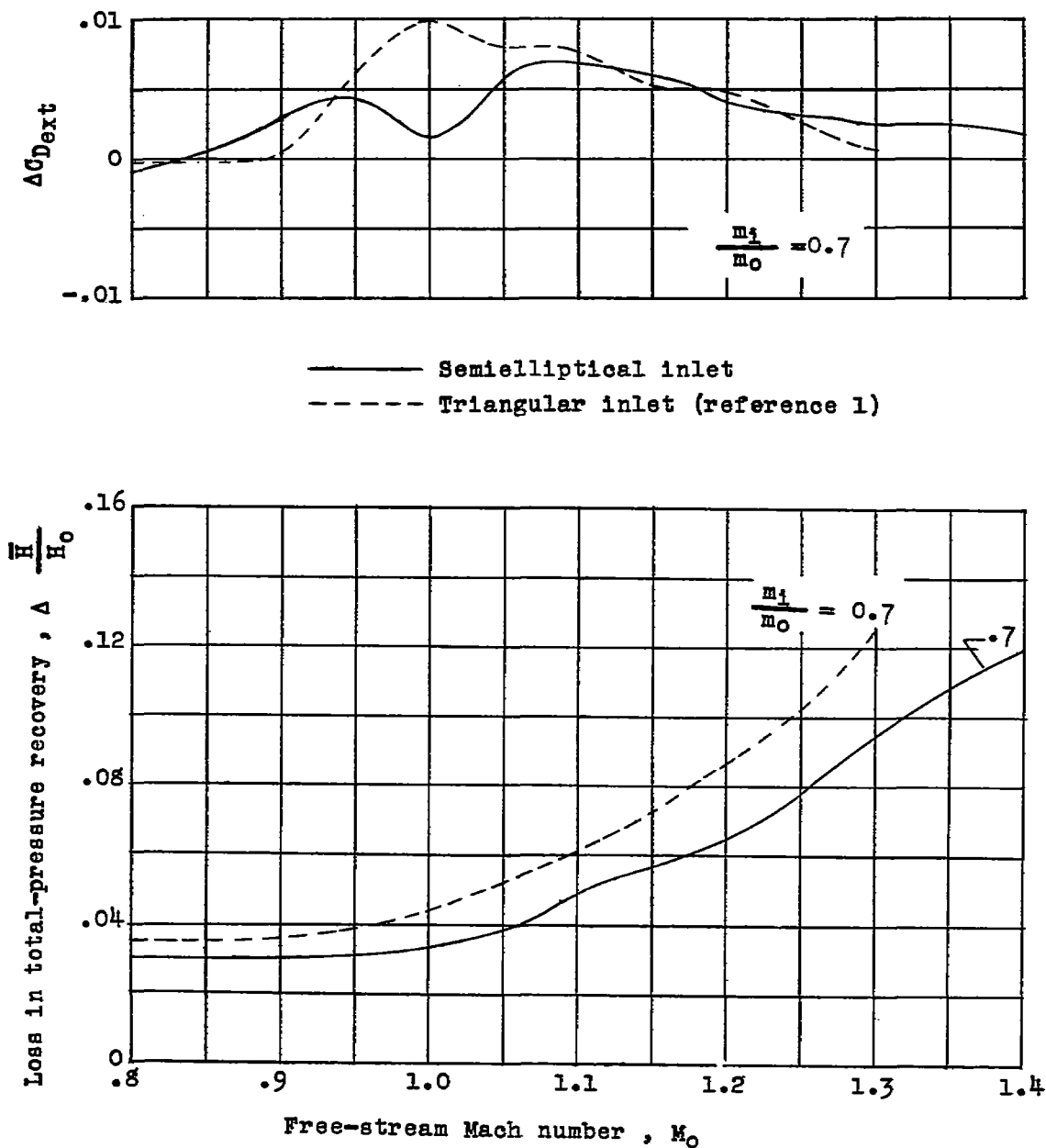


Figure 16.- A comparison of the variation of the external drag increments due to the inlet and the internal total-pressure loss with Mach number for the semielliptical wing-root inlet ( $\alpha = 4.2^\circ$ ) and the triangular wing-root inlet of reference 1 ( $\alpha = 4.4^\circ$ ). No boundary-layer removal.



SECUI

NASA Technical Library



3 1176 01437 5951

ATION

